AFCRL-67-0361

Contract Nr. 61(052)-902

15 April 1967

SCIENTIFIC REPORT NO. 2

# PROPAGATION OF LONG ELECTROMAGNETIC WAVES THROUGH ROCK

1 February 1965 - 1 Feburary 1967

DR. W. BITTERLICH

VLF PROJECT
INNSBRUCK, AUSTRIA



THIS RESEARCH HAS BEEN SPONSORED IN PART BY THE
UNITED STATES GOVERNMENT UNDER CONTRACT 61(052)-902.

## PREFACE

The present report reviews a large part of the results obtained during research work in the LF region which was made by N. N e s s l e r within the framework of the VLF project, Innsbruck.

These studies at high frequencies are an important and essential supplement to the studies on low frequency wave propagation through solid media.

Contractor: Dr. Wolfram BITTERLICH
Kaiser-Franz-Josefstr. 5
A-6o2o Innsbruck, Austria

## ABSTRACT

A description is given of the propagation of long electromagnetic waves through rock, in continuation of our previous studies on the VLF region.

The theoretical bases of wave propagation are reviewed. Important results of comprehensive calculations are summarized and methods of measuring the propagation parameters $\varepsilon$, dielectric constant, and $\sigma$, conductivity, are derived. The instruments used for conducting the measurements are described. Most of them had to be built by our team.

Measurements in the near field and in the near field - far field transition zone as well as through ore beds are evaluated.

TABLE OF CONTENTS


| | page |
|---|---|
| Preface | |
| Abstract | |
| 1. Theory | 1 |
| 2. Apparatus | 7 |
| 2.1 Large transmitting frame SA 10, | 7 |
| 2.2 Battery transmitter, | 8 |
| 2.3 Device for automatic antenna rotation | 8 |
| 2.4 Receiving antenna FA 6 | 9 |
| 2.5 Theory of measurement with the direction-finder antenna | 12 |
| 3. Directivity pattern measurements with the portable transmitter | 16 |
| References | |

## LIST OF ILLUSTRATIONS


Chapter 1: Theory of wave propagation

1.1 General representation SA - EA

1.2 Field line pattern, directivity pattern measurements

1.3 r - $H_r$ diagram, $\sigma$ = parameter, $\nu$ = 120 kc/sec

1.4 r - $H_\varphi$ diagram, $\sigma$ = parameter, $\nu$ = 120 kc/sec

1.5 r - $H_\varphi$ diagram, $\sigma$ = const., $\nu$ = parameter

1.6 2 directivity patterns $\sigma$ = const, r = parameter

1.7 2 directivity patterns, r = const, $\sigma$ = parameter

1.8 r-G diagram, $\sigma$ = parameter, $\nu$ = 120 kc/sec

1.9 r-G diagram, $\sigma$ = parameter, $\nu$ = 10 kc/sec, 1Mc/sec

1.10 $\vartheta$-$\gamma$ diagram, G = parameter

1.11 field line pattern for far field transition, only used in [6]

1.12 $H_\varphi$ -G diagram, $\varepsilon$, $\sigma$ = parameter, 120 kc/sec, 100 m

1.13 $H_\varphi$ -G diagram, $\varepsilon$, $\sigma$ = parameter, 120 kc/sec, 200 m

1.14 $H_\varphi$ -G diagram, $\varepsilon$, $\sigma$ = parameter, 250 kc/sec, 50 m

1.15 $H_\varphi$ -G diagram, $\varepsilon$, $\sigma$ = paramter, 1 Mc/sec , 20 m

Chapter 2: Measuring instruments and devices

2.1 circuit diagram of transmitter

2.2 automatic rotation device, principle

2.3 automatic rotation device, set-up

2.4 automatic rotation device, circuit diagram

2.5 bearing head for FA 6 (schematic)

2.6 receiver preamplifier, circuit diagram

2.9 reception characteristics for rotation field

2.10 rotation field ellipse

Chapter 3: Methods and results of measurement

3.1 miner's map of Gertraudi

3.2 measurement Südost-Morgenschlag $\vartheta = 90^\circ$, using old maps

3.3 measurement Südost-Morgenschlag $\vartheta = 90^\circ$, using new maps

3.4 angular measurement in the mine

3.5 standard measurement at Gertraudi, Südostschlag

3.6 profile measurement Westschlag with diagrams

3.7 directivity patterns Südostschlag using old maps

3.8 Lafatsch I, refraction on the ore blade

3.9 Lafatsch II, map

# PROPAGATION OF LONG ELECTROMAGNETIC WAVES THROUGH ROCK

## 1. Theory

In the reports [1] - [4] only the propagation of very long waves (3 - 30 kc/sec, i.e., 100 - 10 km wavelength in vacuo) through a conductive medium has been described. The effects expected on transition from the near field to the far field could not be studied at these large wavelengths. Neither was the homogeneous and conducting region large enough for this purpose, nor was the power of the transmitter equipped with rotatable antennas sufficiently high.

For the purpose of studying the near field - far field transition zone and for a better understanding of the rock parameters, $\varepsilon$, dielectric constant, and $\sigma$, conductivity, measurements were made at somewhat higher frequencies. Long waves of the 100 kc/sec region were chosen whose mode of propagation can still be compared with that of very long waves, yet they clearly show transition effects at distances that can be reached easily.

As the theory is valid mainly for long and very long waves, the derivation described in detail in [1] and [2] shall not be repeated, only the results will be used.

The following simplifying conditions have been assumed for this purpose: 1. Let the rock be a homogeneous, isotropic and unbounded medium surrounding the transmitting antenna and the receiver.

2. Let the transmitting antenna radiate as a purely magnetic dipole.
3. Let the distance between the transmitter and receiver be so large that transmitter and receiver may be considered as point-shaped.
4. Let the parameters $\varepsilon$, $\sigma$ and $\mu$ decisive for the propagation be constant and independent of

frequency in the region considered.

In continuation of [5] , only the magnetic vector of the electromagnetic field of radiation was measured in experiments, this is why the magnetic components were considered almost exclusively. Let the dipole axis coincide with the z-axis of the specially suited system of spherical coordinates.

With

$m = n \cdot I \cdot F$ ... magnetic moment of the transmitting dipole

n, I, F ..... number of turns, antenna current, area of the transmitting frame

$\vartheta$ ..... angle between the dipole and the radius vector pointing to the point of measurement

r ..... distance transmitter - receiver

$k^*$ ..... complex material constant,

the following relations are valid for the magnetic dipole (cf. Fig. 1.1):

$$\vec{H}_r = m \cdot \cos\vartheta \cdot 2 \cdot e^{-ik^* r} \cdot \left(\frac{1}{r^3} + \frac{ik^*}{r^2}\right) \tag{1}$$

$$\vec{H}_\varphi = 0 \tag{2}$$

$$\vec{H}_\vartheta = m \cdot \sin\vartheta \cdot e^{-ik^* r} \cdot \left(\frac{1}{r^3} + \frac{ik^*}{r^2} + \frac{k^{*2}}{r}\right) \tag{3}$$

$$\left|\vec{H}_r\right| = m \cdot \cos\vartheta \cdot h_r \tag{1a}$$

$$\left|\vec{H}_\vartheta\right| = m \cdot \sin\vartheta \cdot h_\vartheta \tag{3a}$$

With

$$k^* = \sqrt{\omega^2 \varepsilon \varepsilon_0 \mu_0} \cdot \sqrt{1 - \frac{i\sigma}{\omega \varepsilon_0 \varepsilon}} = k_1 - ik_2 \tag{4}$$

we obtain

$$k_1 = \sqrt{\frac{1}{2} \omega^2 \varepsilon_0 \varepsilon \mu_0} \sqrt{1 + \sqrt{1 + \left(\frac{\sigma}{\omega \varepsilon_0 \varepsilon}\right)^2}} \tag{5}$$

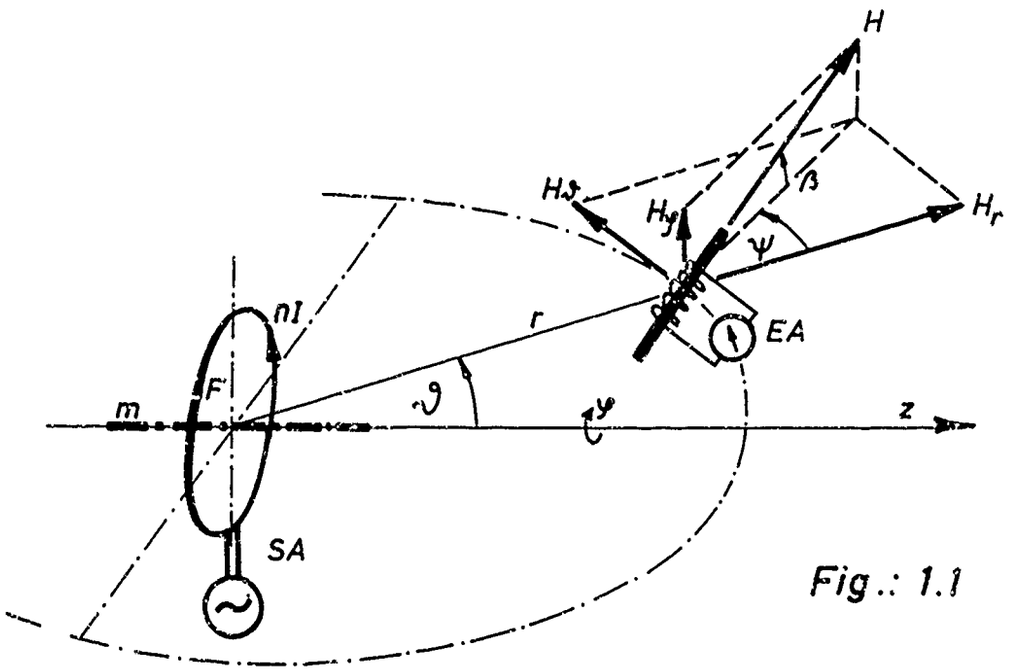
H
Hϑ
Hϕ
Hr
β
ψ
nI
r
EA
F
m
ϑ
ϕ
z
SA

Fig.: 1.1

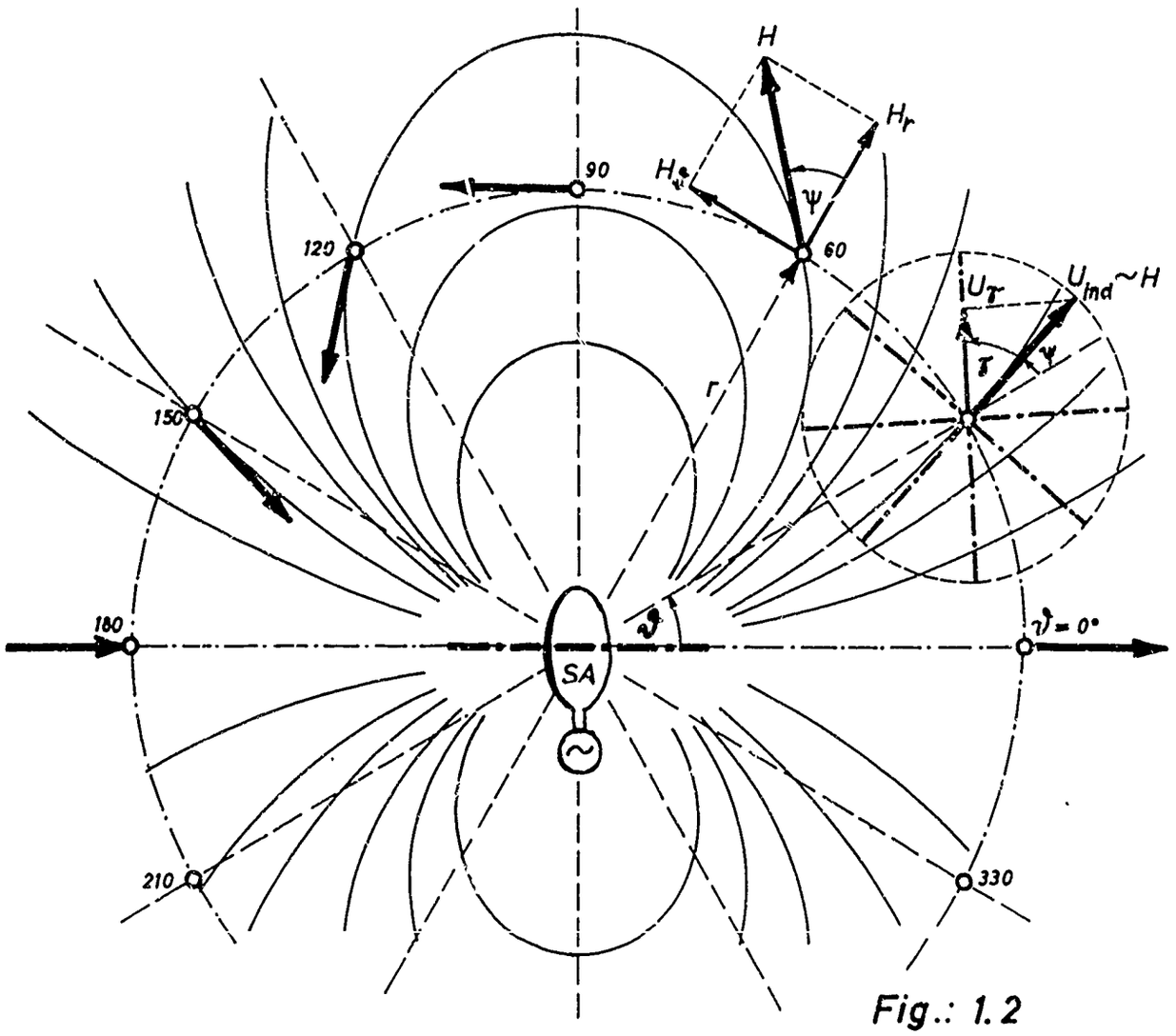
H
Hr
90
Hϑ
ψ
120
60
UT
Uind~H
τ
150
r
180
ϑ
ϑ = 0°
SA
210
330

Fig.: 1.2

and

$$k_2 = \sqrt{\tfrac{1}{2}\omega^2\varepsilon_0\varepsilon\mu_0}\ \sqrt{-1 + \sqrt{1 + \left(\frac{\sigma}{\omega\varepsilon_0\varepsilon}\right)^2}} \quad . \qquad (6)$$

For the simplification $k_1 = k_2 = k$, which is admissible in a wide region of VLF waves, the condition $\sigma/\omega\varepsilon_0\varepsilon \gg 1$ is required. For LF waves, $\omega$ is higher by roughly one power, this is why the above simplification is valid only for very high conductivities. For the theoretical calculation of VLF radiation, the complete expressions of [2] were used.

$\vec{H}_\varphi = 0$ means symmetry about the z-axis (dipole axis) which follows from the geometry of the transmitting antenna considered to be circular. All the field lines thus lie in meridional planes.

Thus the space problem is simplified, the measurement of o n e meridional plane being theoretically sufficient for describing the radiation pattern in full.

Only the value of the field strength (consisting of $\vec{H}_r$ and $\vec{H}_\vartheta$) at the respective point of measurement can be measured. The voltage $U_{ind}$ induced in the coil of the receiving antenna is measured, which is proportional to the amount of the field strength.

$$U_{ind} \sim |\vec{H}| \sim \left\{h_r^2 \cdot \cos^2\vartheta + h_\vartheta^2 \cdot \sin^2\vartheta\right\}^{1/2} \quad . \qquad (7)$$

The direction of the field strength maximum according to Fig. 1.2 is obtained from (7):

$$\tan\psi = \frac{|\vec{H}_\vartheta|}{|\vec{H}_r|} \quad . \qquad (8)$$

Similar to the Gaussian positions, the measurements for $\vartheta = 0^\circ$ and $\vartheta = 90^\circ$ are of special interest.
Eq. (7) yields

$$\vec{H}\big|_{\vartheta = 0^\circ} \sim h_r \quad (= H_0) \qquad (9)$$

$$\vec{H}\big|_{\varphi = 90^\circ} \sim h_\varphi \ ( = H_{90}) \qquad (10)$$

and

$$G = \frac{h_r}{h_\varphi} \quad . \qquad (11)$$

The latter quantity permits interesting conclusions on the rock parameters.

These expressions were used for computing and tabulating a great number of field strength values by a ZUSE Z 23 computer (program, description and flux diagrams as well as the results will be given in a separate report).

On the basis of these results, the most important relations were represented graphically for the frequency region of 120 kc/sec which was of greatest interest in this connection.

Figs. 1.3 and 1.4 show the relation between the distance r and the field strengths $H_r$ and $H_\varphi$ corresponding to a profile measurement for the Gaussian positions. The variable parameter is the conductivity of the surrounding medium. The frequency of 120 kc had been chosen in accordance with the actual measurements. This representation shows that the dependence of the field strength on conductivity at decreasing distances vanishes (fusion of all the curves into a flat straight line). In the above region only the term with $1/r^3$ is effective (cf. Eqs. (1) and (3)), the term for the exponential attenuation becomes unit.

The family of curves splits up as r increases, at first for higher conductivities, then as the distance becomes larger still, also for lower conductivities. The steeper drop of curves represents the influence of the exponential attenuation. The two curves for $H_r$ and $H_\varphi$ corresponding to the Gaussian positions 0 and $90^\circ$ differ in that the initial value of $H_\varphi$ is half that of $H_r$, and that $H_\varphi$ has a relative maximum. Thus, the curve for a certain value of r and $\sigma$ rises above the other family of curves and drops exponentially as the distance increases. From hereon, however, the

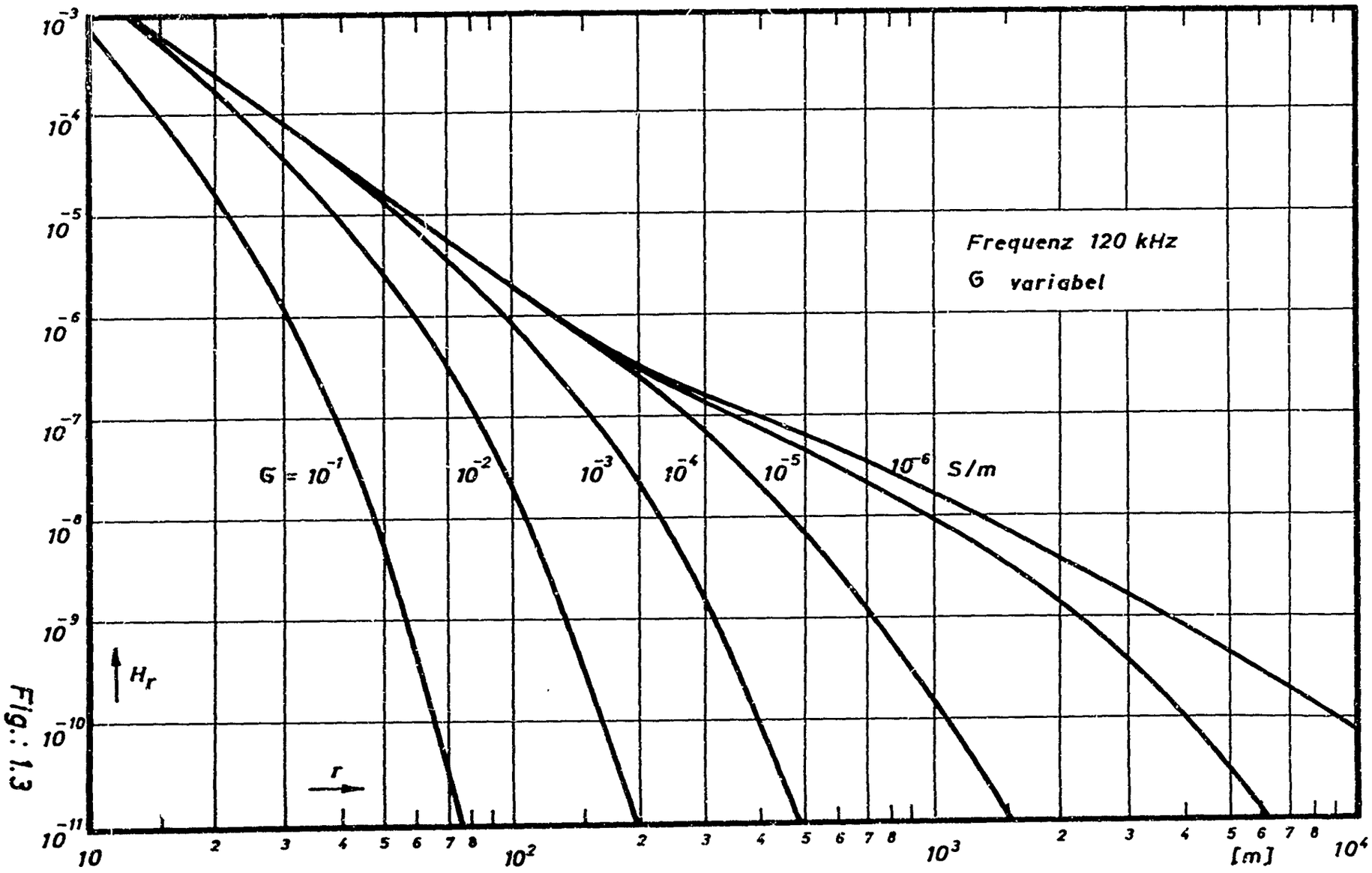
Frequenz 120 kHz
G variabel
G = 10^-1
10^-2
10^-3
10^-4
10^-5
10^-6 S/m
H_r
r
[m]
10^-3
10^-4
10^-5
10^-6
10^-7
10^-8
10^-9
10^-10
10^-11
10
10^2
10^3
10^4

Fig.: 1.3

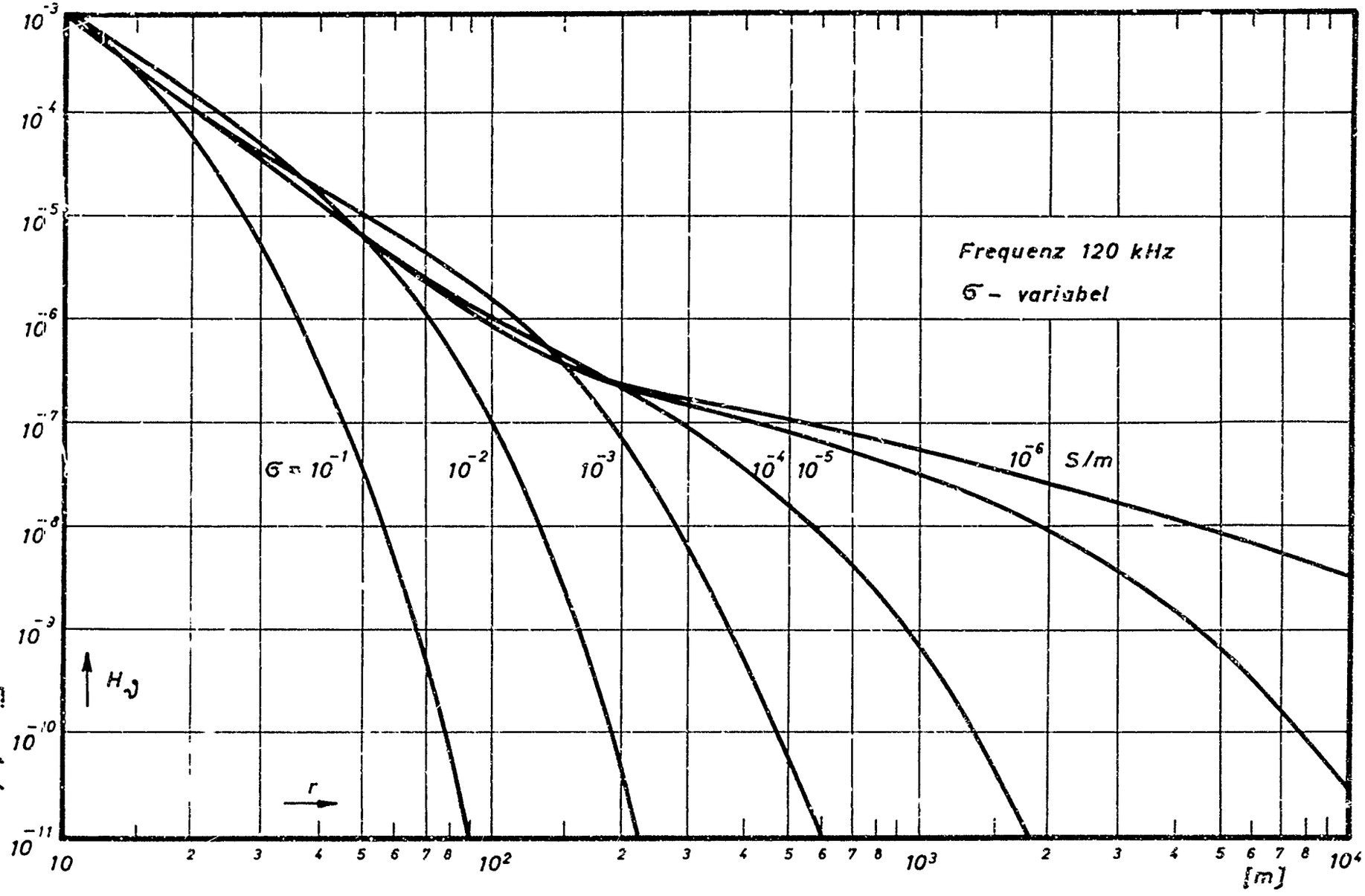


Fig.: 1.4

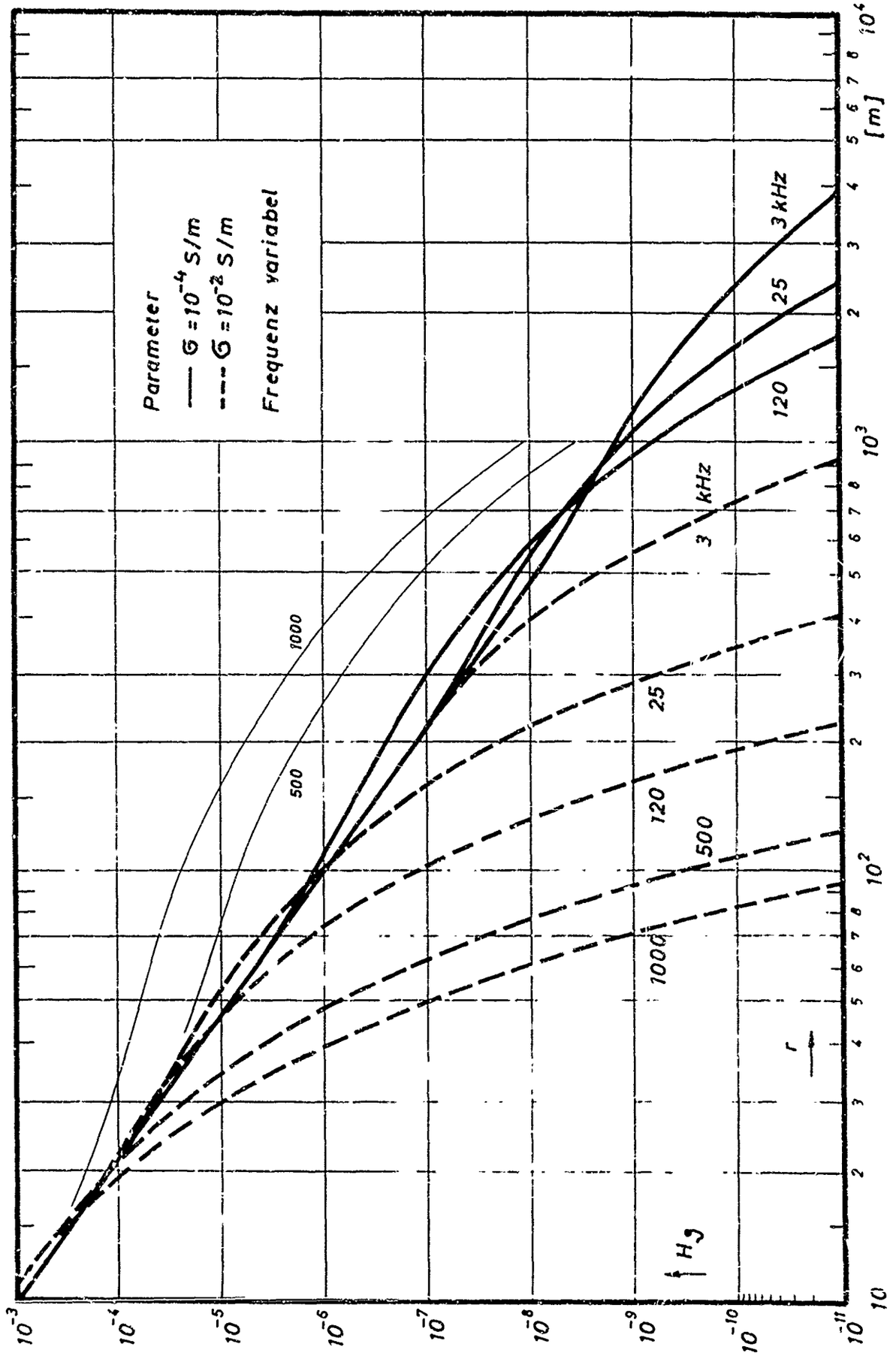
Parameter
— σ = 10⁻⁴ S/m
--- σ = 10⁻² S/m
Frequenz variabel
3 kHz
25
120
500
1000
r [m]
H

Fig.: 1.5

exponential attenuation by far exceeds the small decrease proportional to 1/r which in the expression in brackets (cf. (3)) represents the most important term at large distances.

The family of curves represented in Fig. 1.5 similarly to Fig. 1.4 shows the dependence of $H_\vartheta$ on r, the parameter being the frequency, and the conductivity being kept constant. This representation illustrates the greater attenuation at higher frequencies. If the frequency can be chosen, it should be adapted to the physical conditions, depending on the purpose of this experiment. For a direction-finding measurement largely undisturbed by the surrounding medium, the chosen frequency should be as low as possible, whereas for determining the rock parameters and ore inclusions of different conductivity it should be as high as possible. The upper limit is given by the attenuation of the distance to be covered.

Another important and frequently used type of measurement through a medium is illustrated by the directivity patterns of Figs. 1.6 and 1.7. Fig. 1.6 shows the change in directivity pattern for conductivities of $10^{-4}$ and $10^{-2}$ mhos/m at increasing distance. The change from a horizontal figure of eight to a circle and vertical figure of eight corresponds to the attenuation which is higher for $H_r$ than for $H_\vartheta$. The field strength values $H_0$, $H_{30}$, $H_{60}$, $H_{90}$ are plotted on a linear scale from the center at the corresponding angles of $\vartheta$. In view of a good graphical representation, a separate scale of the field strength was required for each distance (a logarithmic scale would be meaningless in a circular diagram).

A directivity pattern having the shape of the diagram in Fig. 1.7 can be used for determining the conductivity. At a given frequency and distance, the shape of the directivity pattern and the ratio between $H_0$ and $H_{90}$ is a measure of conductivity. As the quotient of two similar measurements is used for the determination, this measurement is independent of all calibration fields,

i.e., it can be made without an absolute calibration. The relation between r and $G = H_0/H_{90}$ (cf. Eq.(11)) as dependent on the frequency and conductivity is shown in Figs. 1.8 and 1.9. The maximum which cannot be recognized from the equation and which occurs at a certain combination of conductivity and distance is of interest, with the function G approaching the value of 3. Below the dashed line of $G = 1$, the curves are linear. From a value of $G > 1$ onward, we may speak in terms of the far field.

When measuring a directivity pattern, the angle $\psi$ between receiving antenna and radius vector also changes in dependence on the structure of the field line pattern (Fig. 1.2). The relation between $\psi$ and the other quantities is expressed in the following equation:

$$\tan\psi = \frac{h_\vartheta \cdot \sin\vartheta}{h_r \cdot \cos\vartheta} = \frac{\tan\vartheta}{G} \quad . \tag{12}$$

The dependence of the angle $\psi$ on $\vartheta$ is shown in the diagram of Fig. 1.10 for various G values.

For the diagrams shown so far, a dependence on the dielectric constant $\varepsilon$ was neglected. For studying in detail the wave propagation in a medium, all decisive parameters must be known. In the diagrams 1.11 - 1.14, where $H_\vartheta$ and G are the abscissa and ordinate, respectively, families of curves are plotted whose constant parameters are $\varepsilon$ and $\sigma$, with one diagram being valid for one certain distance. All these diagrams show that various $\varepsilon$ values can be distinguished only below a certain conductivity. A comparison between Figs. 1.11 and 1.12 - 1.14 shows that the curves split up at higher frequency already at very low distance.

These diagrams are of great practical importance, since from two quantities measured at one point of reception, conclusions can be made as to the two decisive parameters $\sigma$ and $\varepsilon$.

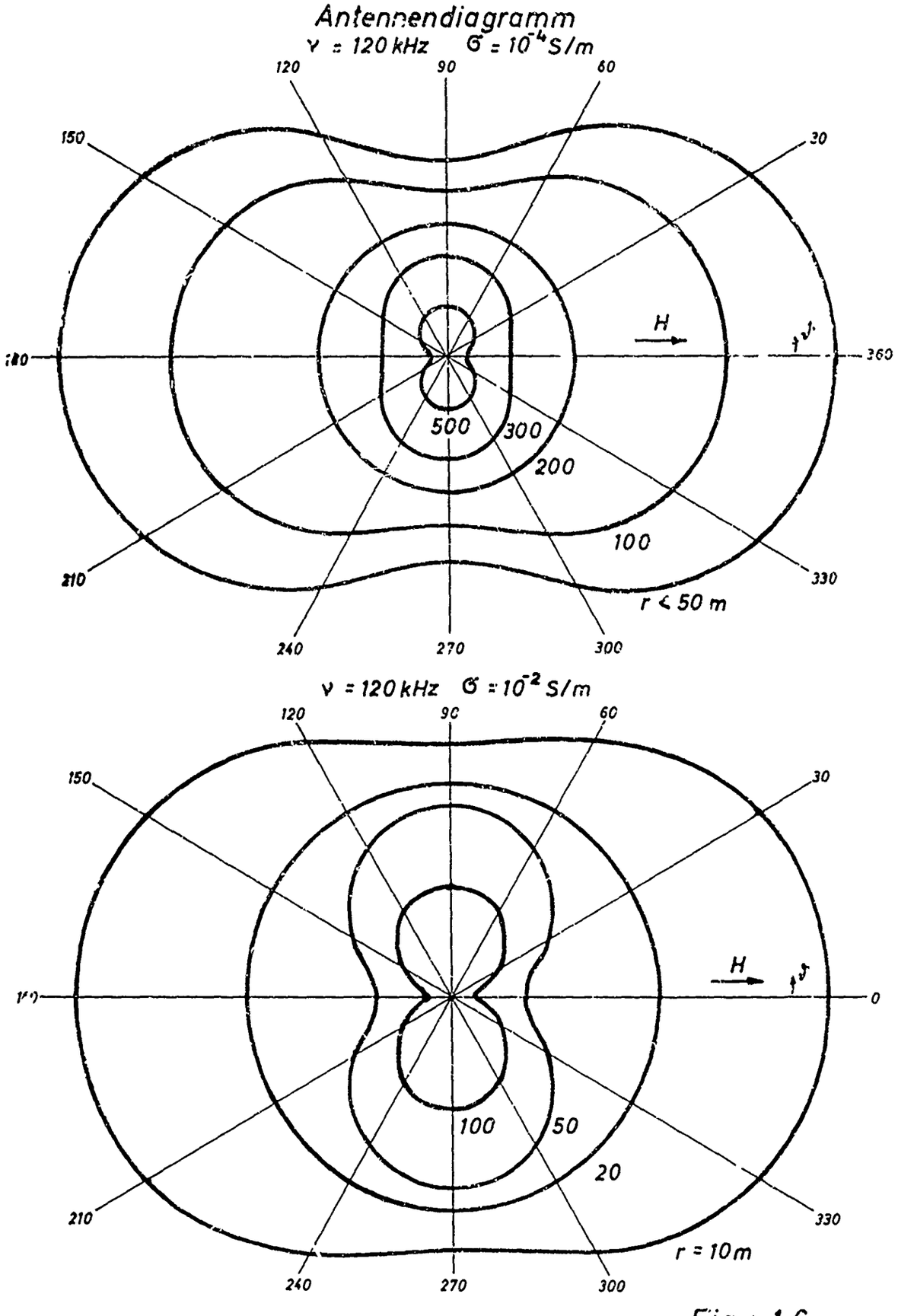
Antennendiagramm
ν = 120 kHz σ = 10⁻⁴ S/m
120
90
60
150
30
180
360
H
500
300
200
100
210
330
r < 50 m
240
270
300
ν = 120 kHz σ = 10⁻² S/m
120
90
60
150
30
H
0
100
50
20
210
330
r = 10m
240
270
300

Fig.: 1.6

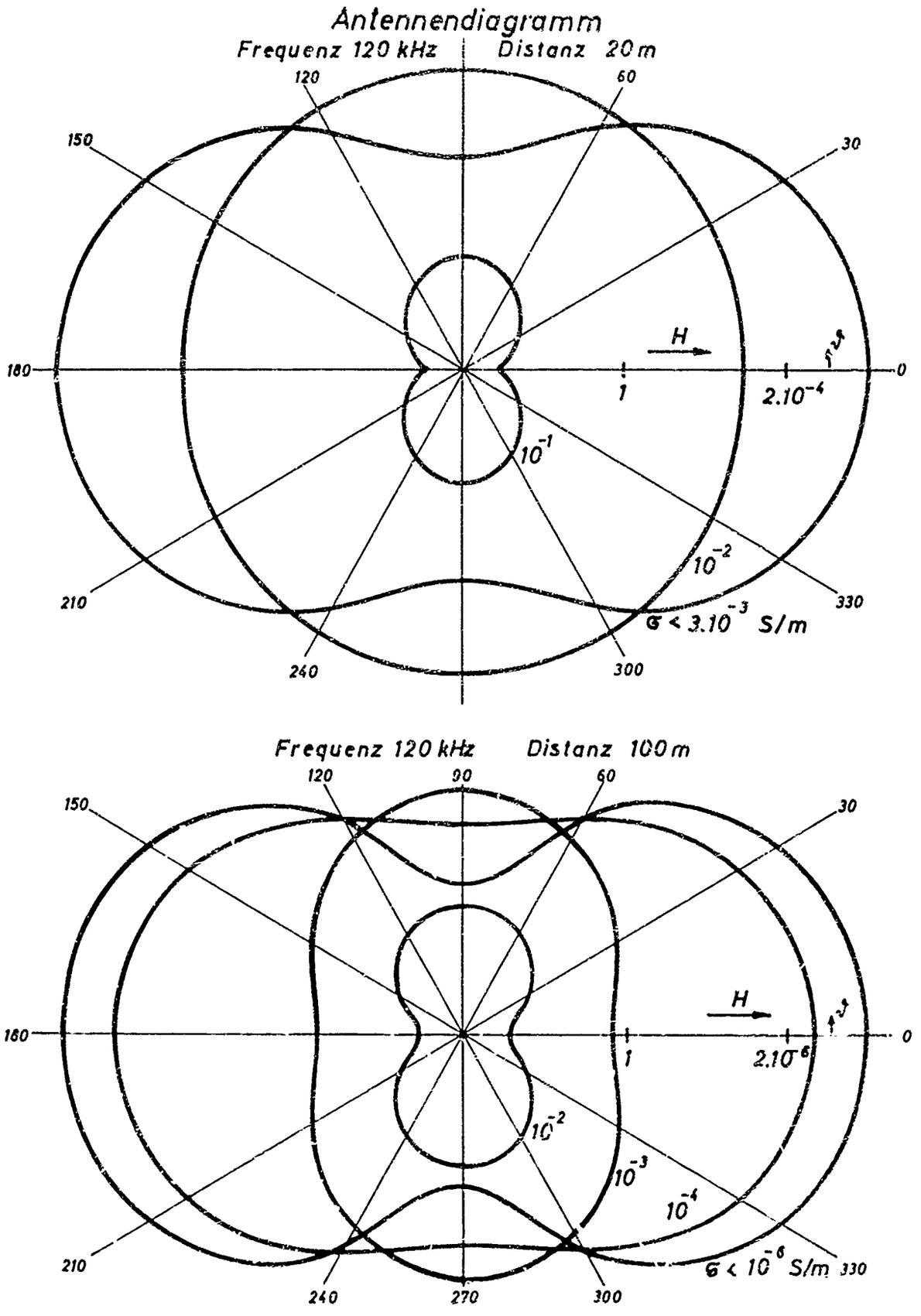
Antennendiagramm
Frequenz 120 kHz
Distanz 20 m
120
60
150
30
180
0
H
1
2.10⁻⁴
10⁻¹
10⁻²
210
330
σ < 3.10⁻³ S/m
240
300
Frequenz 120 kHz
Distanz 100 m
120
90
60
150
30
180
0
H
1
2.10⁻⁶
10⁻²
10⁻³
10⁻⁴
210
330
σ < 10⁻⁶ S/m
240
270
300

Fig.: 1.7

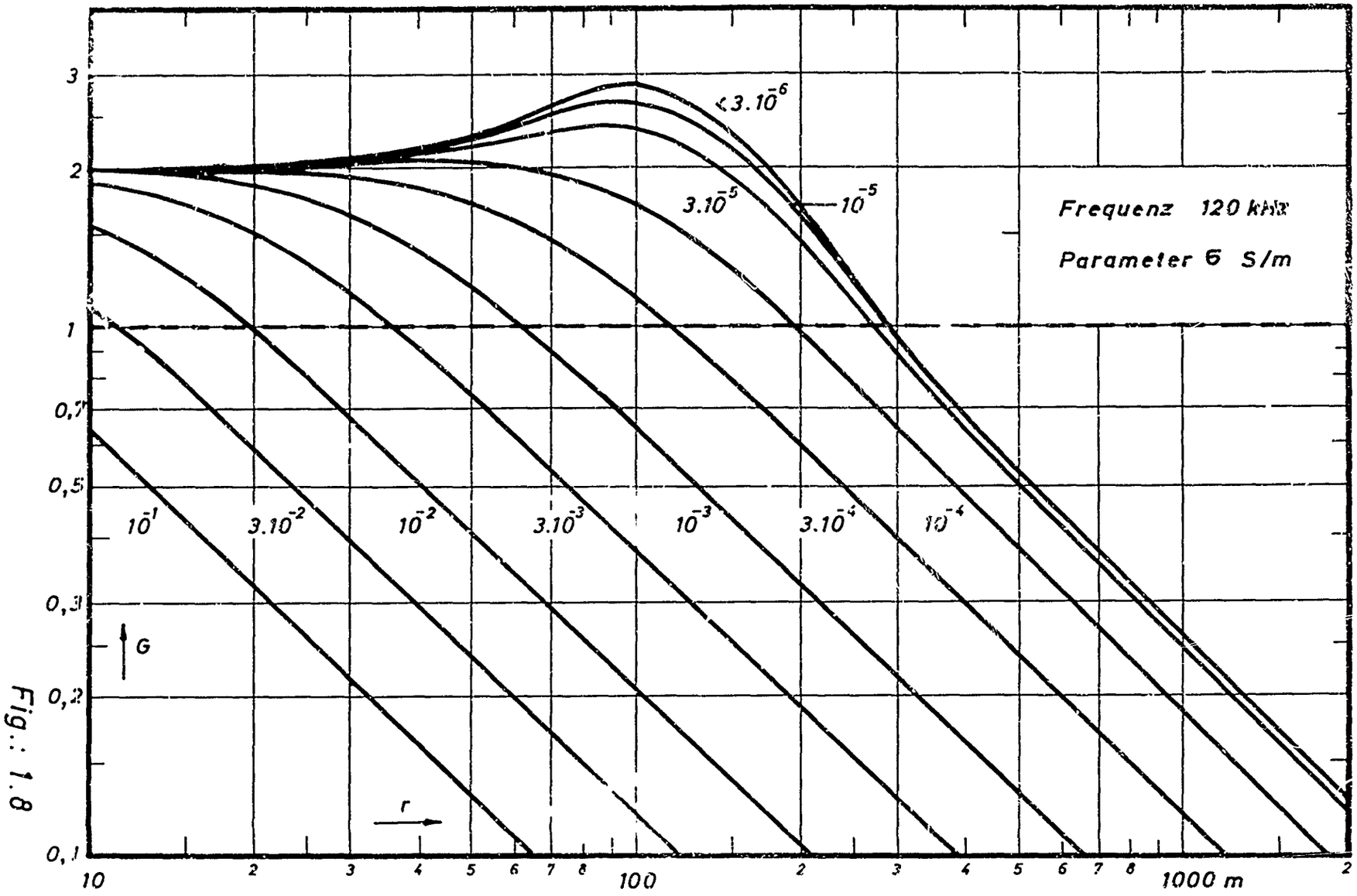
Frequenz 120 kHz
Parameter G S/m
< 3.10⁻⁶
3.10⁻⁵
10⁻⁵
10⁻¹
3.10⁻²
10⁻²
3.10⁻³
10⁻³
3.10⁻⁴
10⁻⁴
G
r
3
2
1
0,7
0,5
0,3
0,2
0,1
10
100
1000 m

Fig.: 1.8

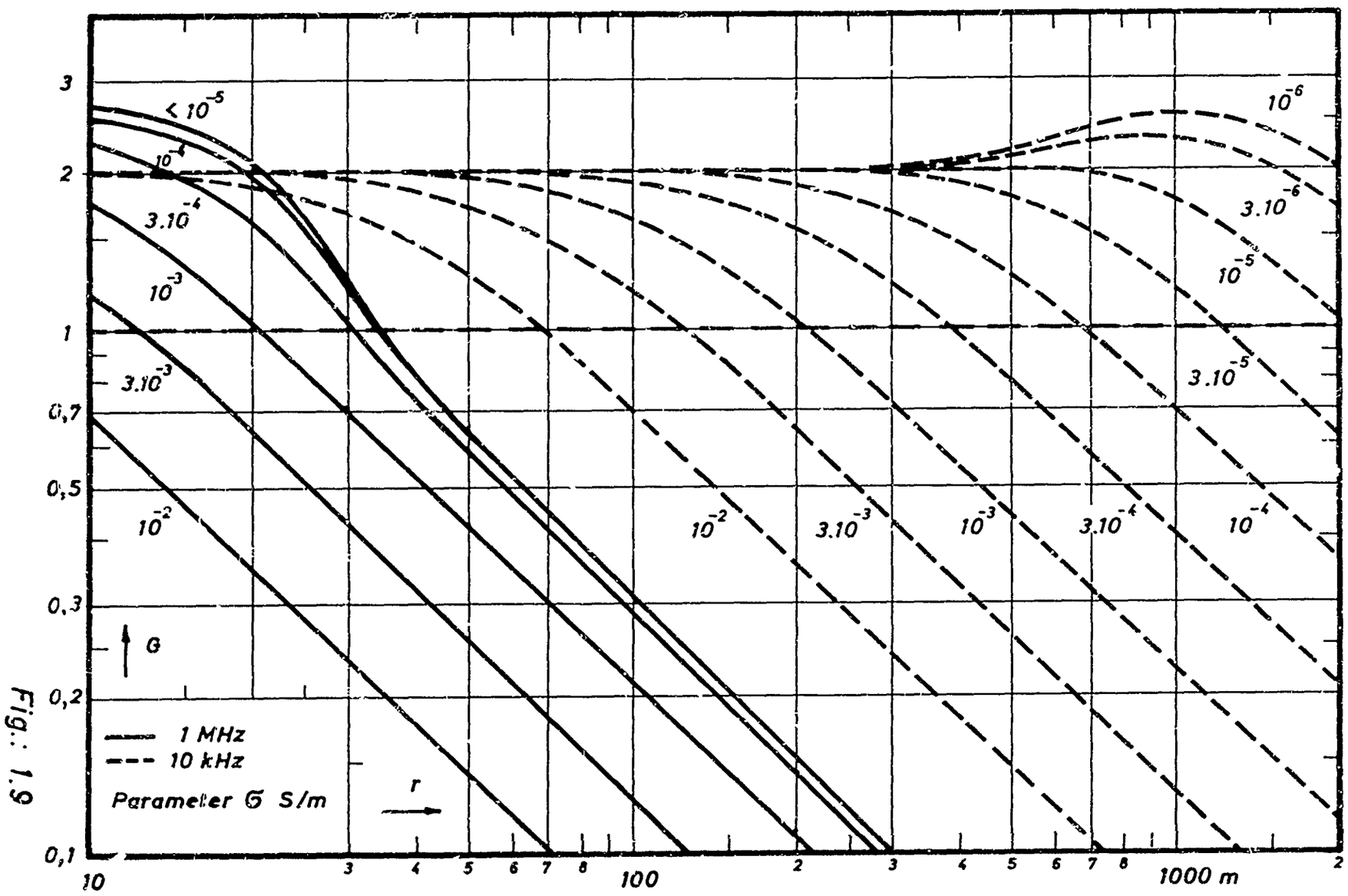
3
2
1
0,7
0,5
0,3
0,2
0,1
10
100
1000 m
< 10⁻⁵
10⁻⁴
3.10⁻⁴
10⁻³
3.10⁻³
10⁻²
10⁻⁶
3.10⁻⁶
10⁻⁵
3.10⁻⁵
10⁻²
3.10⁻³
10⁻³
3.10⁻⁴
10⁻⁴
G
1 MHz
10 kHz
Parameter σ S/m
r

Fig.: 1.9

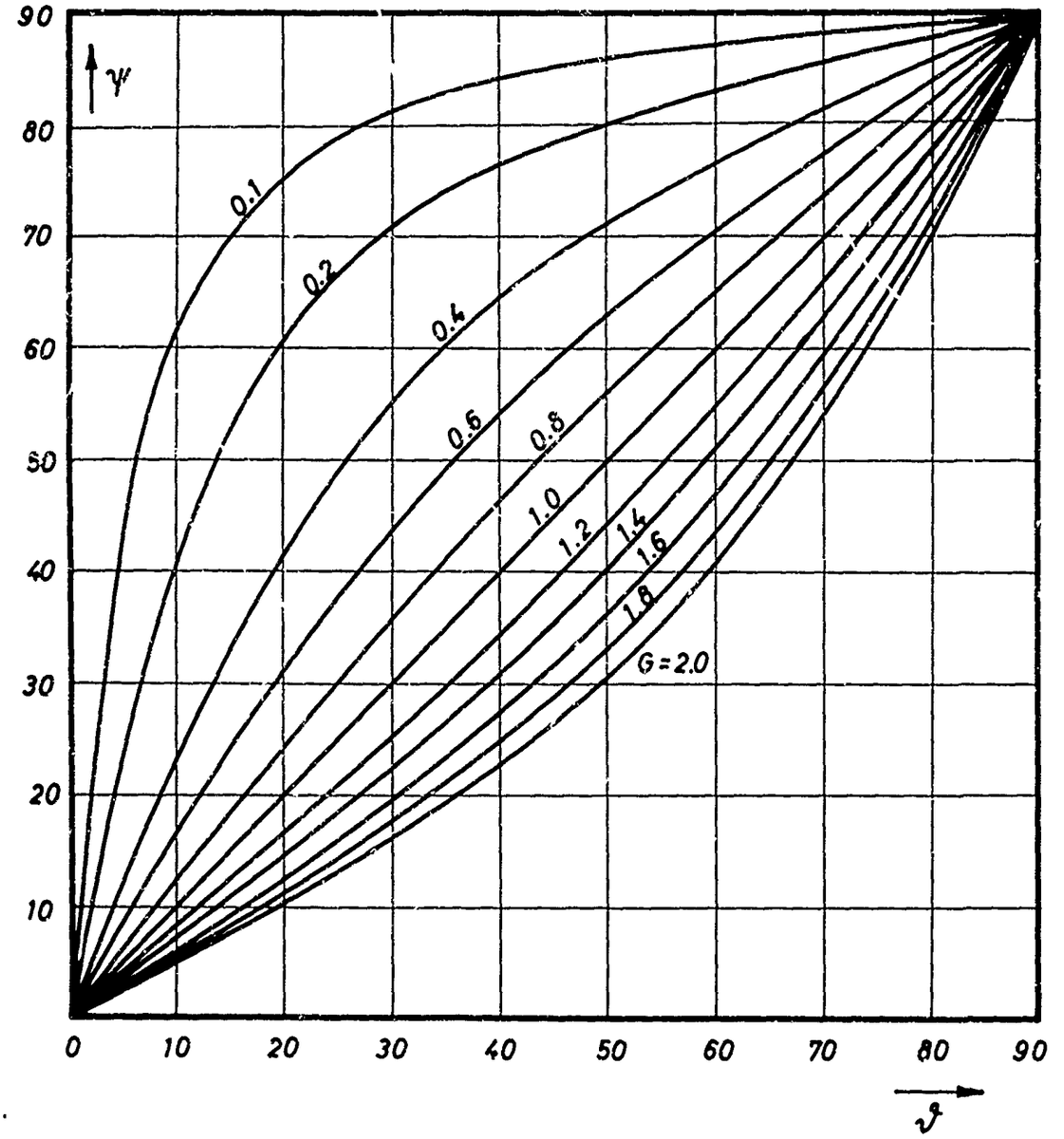


$$tg\,\psi = \frac{tg\,\vartheta}{G}$$

Fig.: 1.10

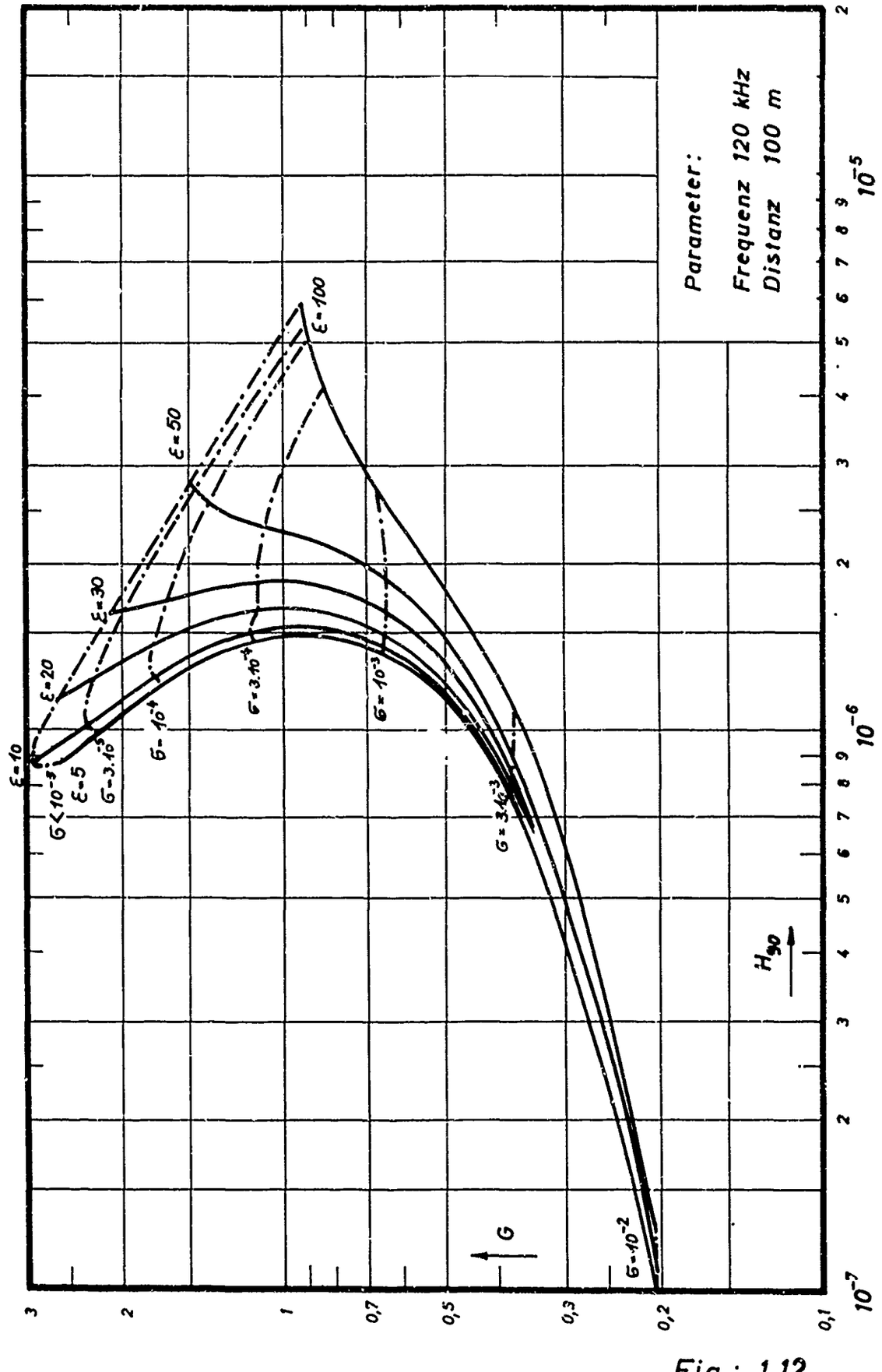
Parameter:
Frequenz 120 kHz
Distanz 100 m
ε=100
ε=50
ε=30
ε=20
ε=10
ε=5
G<10⁻⁵
G=3.10⁻⁵
G=10⁻⁴
G=3.10⁻⁴
G=10⁻³
G=3.10⁻³
G=10⁻²
G
H90
10⁻⁵
10⁻⁶
10⁻⁷
3
2
1
0,7
0,5
0,3
0,2
0,1

Fig.: 1.12

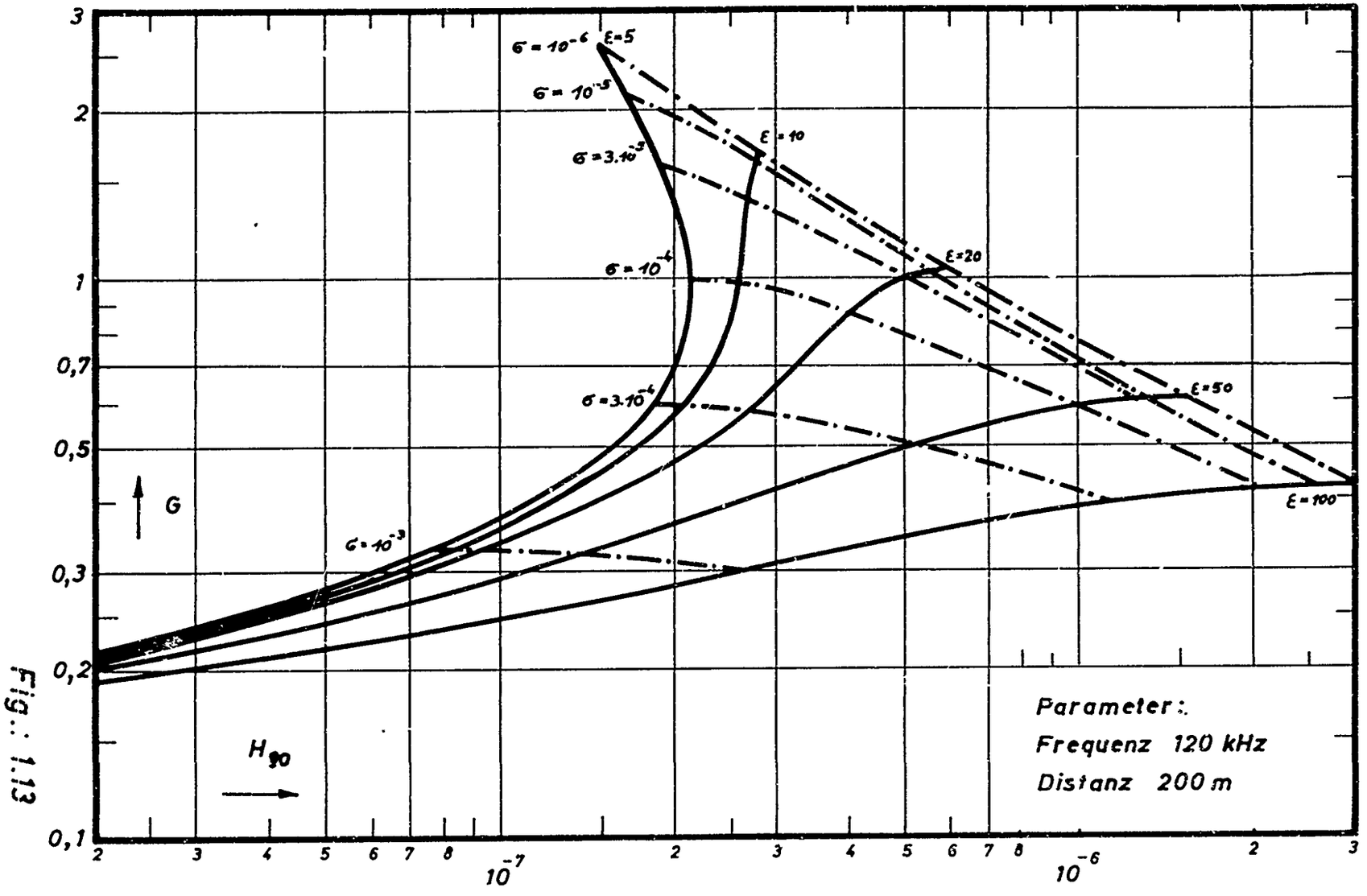
σ = 10⁻⁶
ε=5
σ = 10⁻⁵
ε = 10
σ = 3.10⁻⁵
σ = 10⁻⁴
ε=20
σ = 3.10⁻⁴
ε=50
σ = 10⁻³
ε = 100
G
H90
Parameter:
Frequenz 120 kHz
Distanz 200 m
10⁻⁷
10⁻⁶

Fig.: 1.13

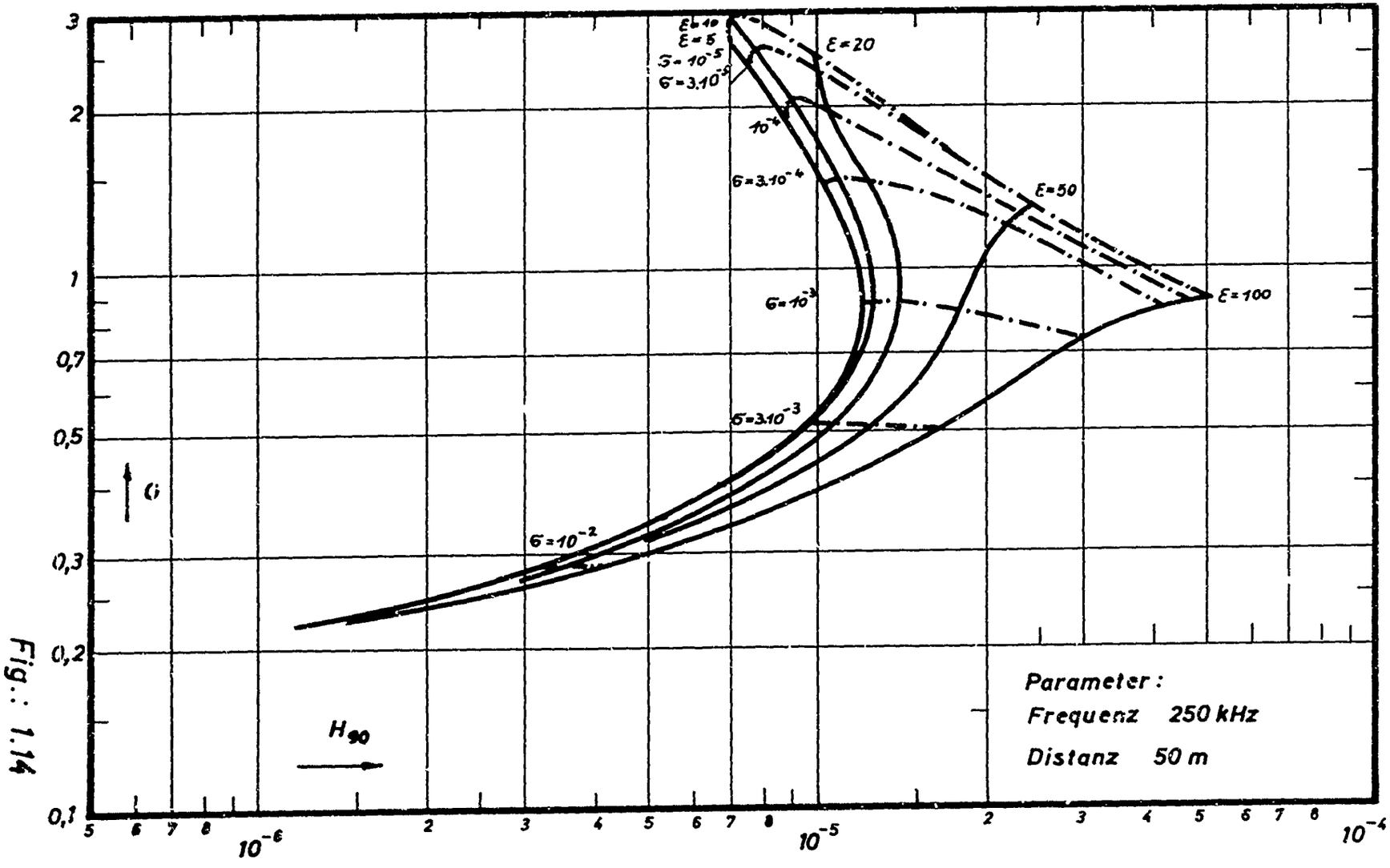
3
2
1
0,7
0,5
0,3
0,2
0,1
G
$H_{90}$
$10^{-6}$
$10^{-5}$
$10^{-4}$
ε=10
ε=5
σ=10⁻⁵
σ=3.10⁻⁵
ε=20
10⁻⁴
σ=3.10⁻⁴
ε=50
σ=10⁻³
ε=100
σ=3.10⁻³
σ=10⁻²
Parameter:
Frequenz 250 kHz
Distanz 50 m

Fig.: 1.14

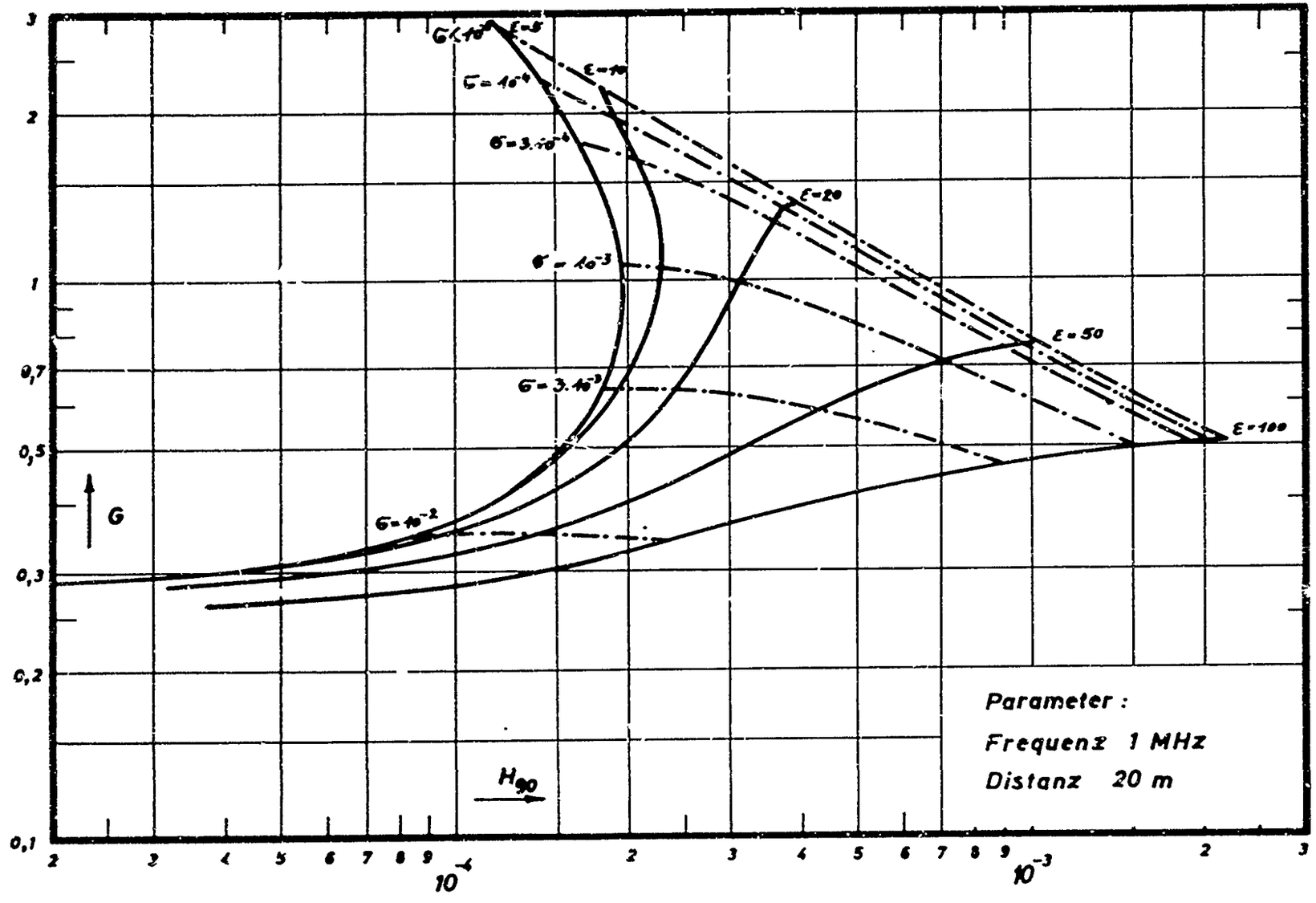
G
$H_{90}$
$10^{-4}$
$10^{-3}$
$\sigma = 10^{-2}$
$\sigma = 3.10^{-2}$
$\sigma = 10^{-3}$
$\sigma = 3.10^{-3}$
$\sigma = 10^{-4}$
$\varepsilon = 5$
$\varepsilon = 10$
$\varepsilon = 20$
$\varepsilon = 50$
$\varepsilon = 100$
Parameter :
Frequenz 1 MHz
Distanz 20 m

Fig.: 115

## 2. Apparatus

Transmitters and receivers for the LF region were designed and built on the basis of experience made when constructing transmitters and receivers for VLF waves (for details see [2], [3] and [4]). [6] gives a detailed description.

### 2.1 Large transmitting frame SA 10, Fig. I

The dimensions of the new frame (4 x 4 m) were given by the size of the cavity in the mine, furthermore the antenna had to be rotatable through an angle of at least 180° for the purpose of measuring the antenna diagram. The theoretical considerations in [1] showed that the radiation of frame coils free of iron is better than that of coils filled with iron or ferrite.

Because of the calculated weight of approximately 80 kg, a strong roof structure made of aluminum angle sections (40 x x 40 x 5 mm) was pivoted on a thrust ball bearing. The frame is fed from the laboratory to the first turn via Lecher wires, by means of a transmitter (Type Aeronautical Communications Equipment Inc., Model 12 GLX-M, Serial Nr. 312). The antenna is tuned to resonance by means of capacitors. The resonance current in the antenna has a maximum of 3.4 a, the resonance voltage was approximately 13.000 $v_{pp}$. This transmitter was used for a great number of measurements in the mine of Großkogel.

As the transmitter was connected galvanically with the wide network of rails (grounding), the electrical conditions were complicated and therefore their evaluation cannot be given in this report (for details see [6]). The present report is confined to a description of the results measured with a portable transmitter. The portable device is superior to the stationary one in so far as it permits measurements in geologically different regions. Its drawback of a shorter range is thus largely compensated.

2.2 Battery transmitter, Fig. II

The transmitter was designed as a portable unit to be used in various regions. The current source was a 12 v battery, the entire transmitter was fully transistorized. Fig. 2.1 shows the circuit diagram of the transmitter. For a detailed description see [6].

The transmitting antenna SA 11 was designed for the special use with the portable transmitter. The frame construction clearly visible in Fig. II is collapsible. The antenna is tuned to resonance; the power transferred from the transmitter to the antenna is calculated tc be 5.4 watts.

2.3 Device for automatic antenna rotation

For the purpose of measuring the directivity patterns described in Chapter 1, the transmitting antenna had to be rotated about a vertical axis through angles of 15 and 30° at brief intervals of time. A device that turns the antenna automatically had to be designed for the purpose of replacing another assistant for these measurements. The following requirements were made:

a) The SA must be rotatable about the vertical axis through 15° and 30°. Its axis must always remain horizontal (absolute angular deflection error less than 1°).
b) The antenna must be rotated automatically at equal time intervals (adjustable between 3 and 10 minutes, accuracy approximately ± 10 seconds).
c) After a rotation through 180° (occasionally 90° or 360°), the direction of rotation must reverse automatically, the standstill in the final position being 10 - 30 minutes (time for two measurements plus time for walking to another site of measurement, accuracy ± 1 minute).
d) The process of rotation must be signalled at the point of reception.

The device shown in Figs. 2.2 - 2.4 meets these require-

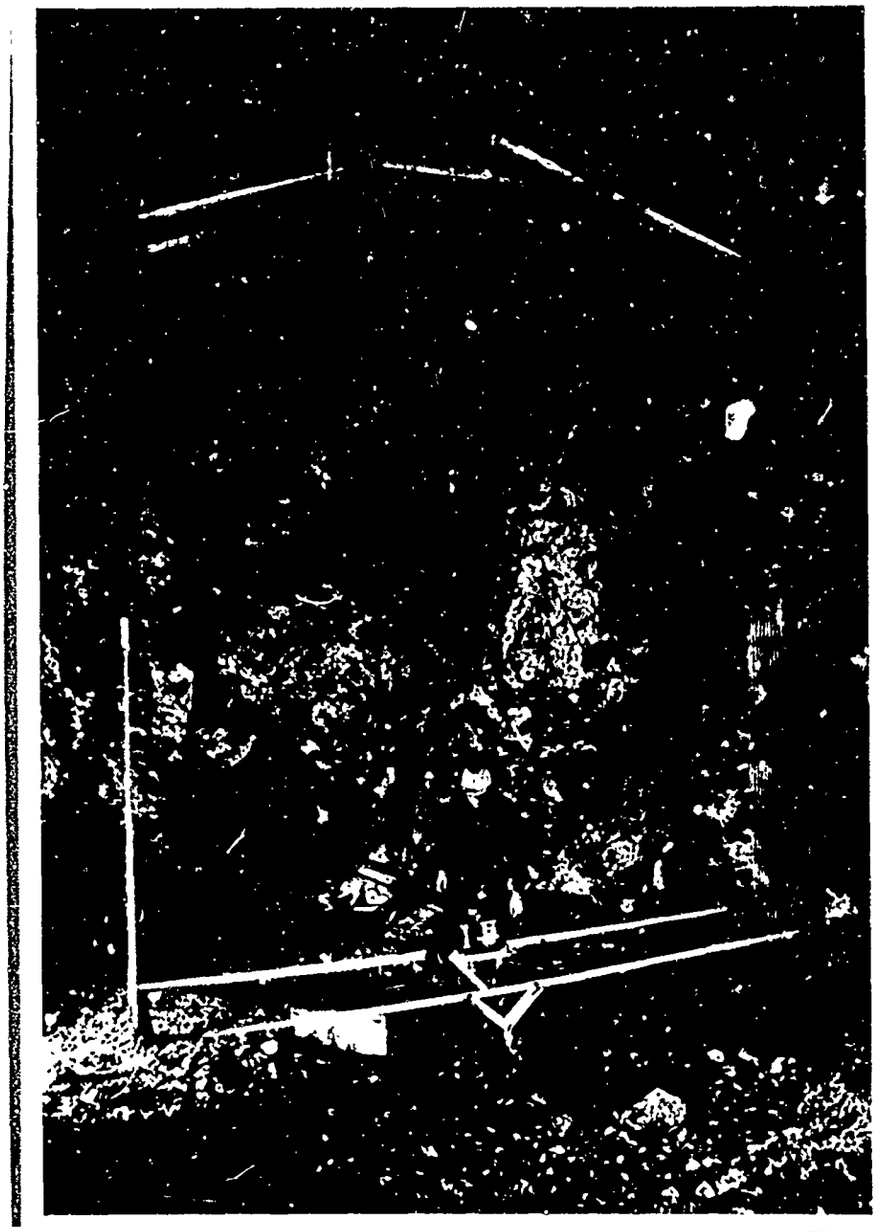

Fig. I

Large transmitting frame SA 10 suspended rotatable in the "Bunte Kluft" in the Großkogel mine, St. Gertraudi; the tuning unit can be seen at the bottom, right above the tappings. To the left is the connection (Lecher wires) with the transmitter.

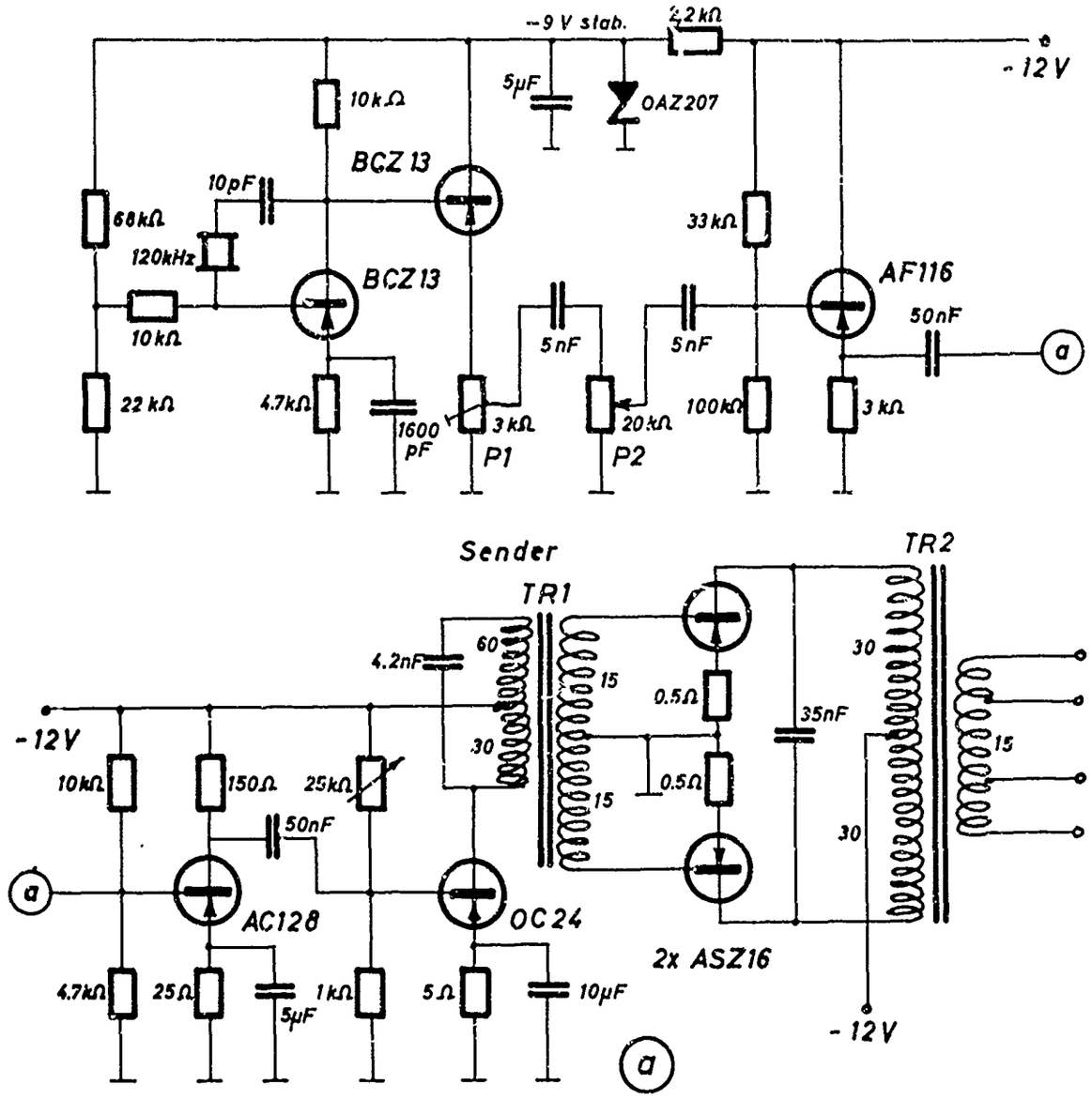


Sender

Fig.: 21

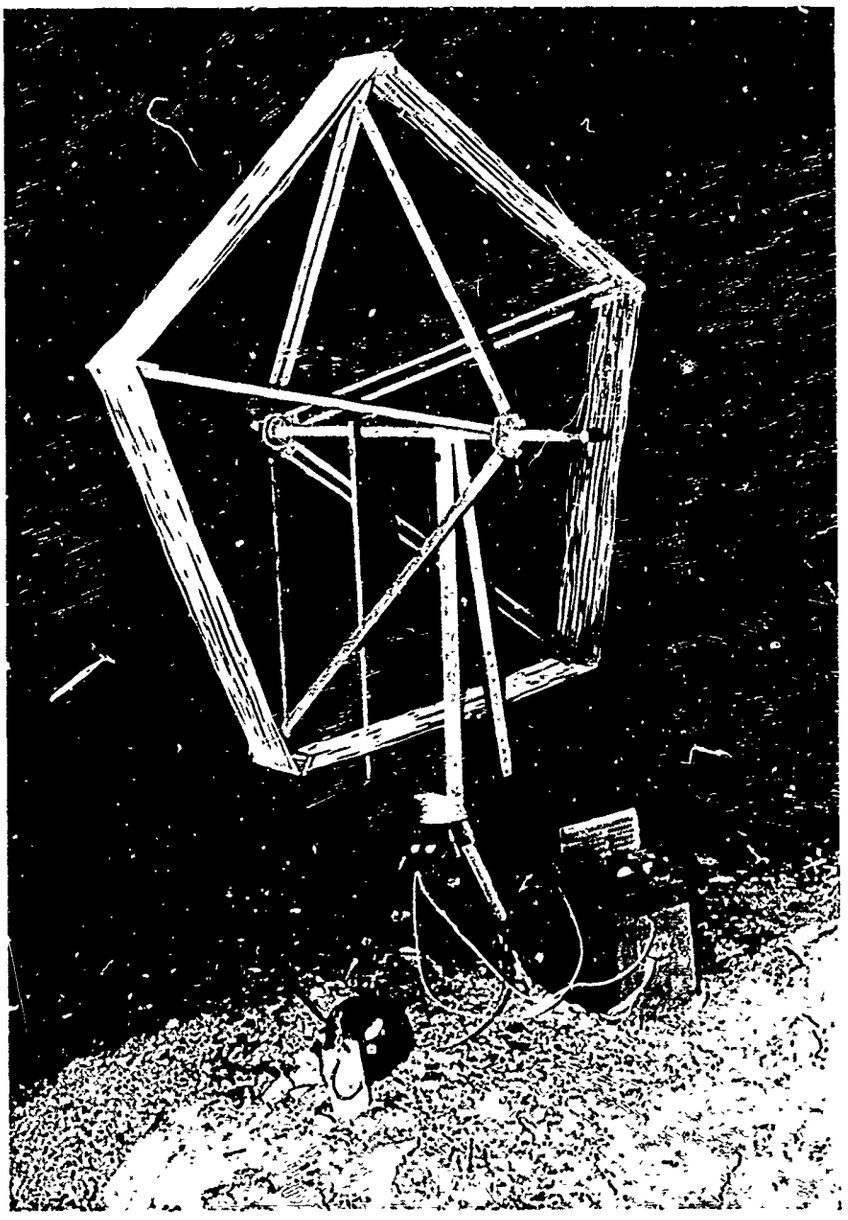

Fig. II

Portable transmitting frame SA 11 with automatic antenna rotation device (below the frame), to the right is the transmitter and tuning unit with instrument on the battery box.

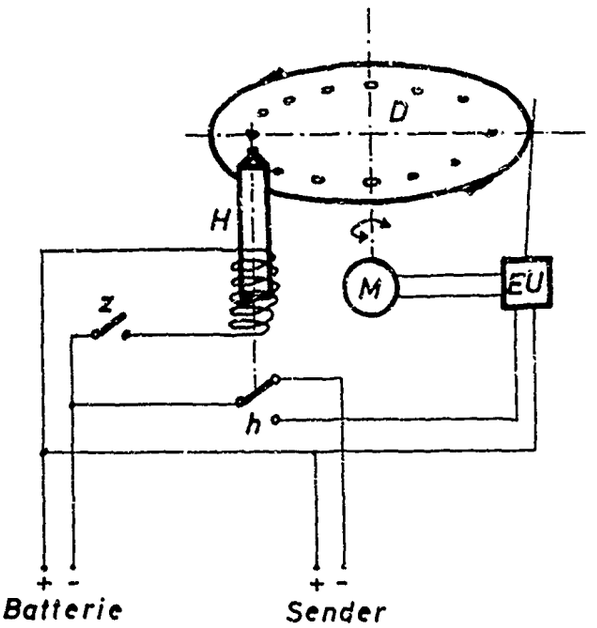


Prinzip

Fig.: 2.2

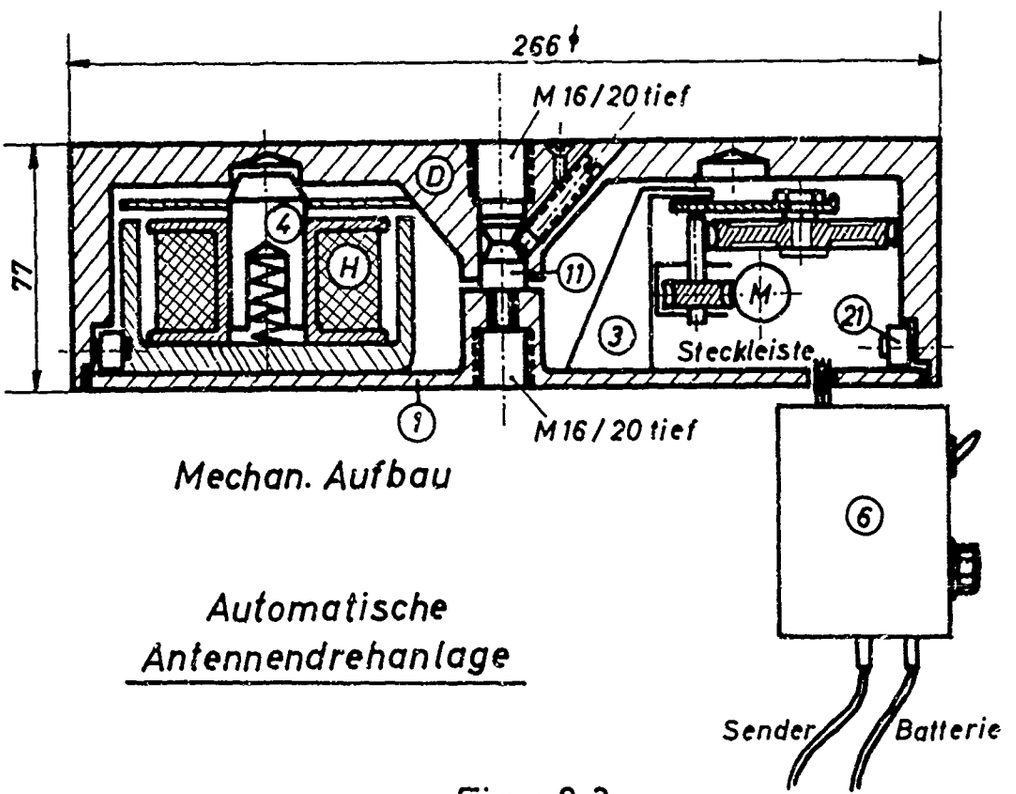


Mechan. Aufbau

Automatische
Antennendrehanlage

Fig.: 2.3

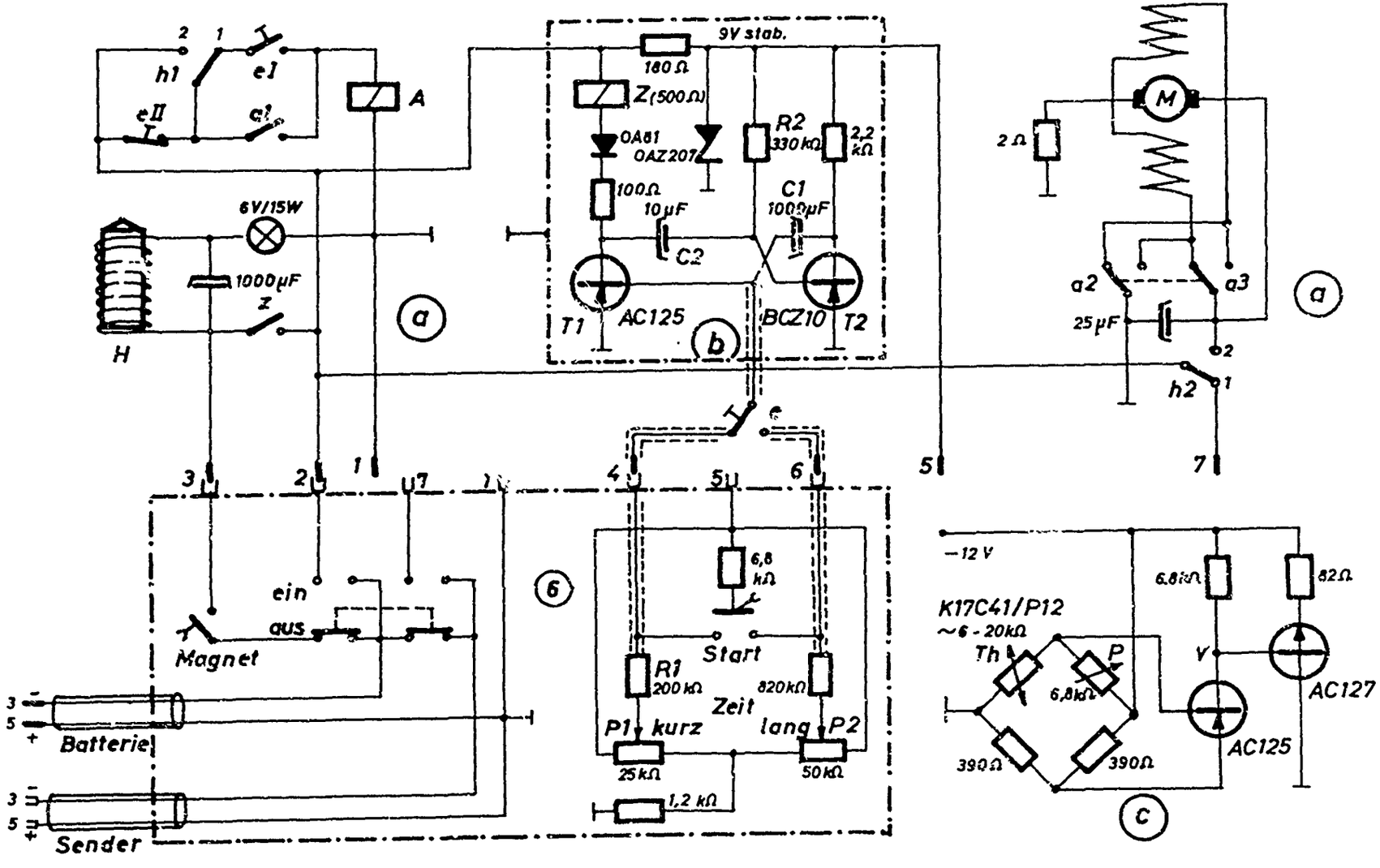


Fig.: 2.4

**Antennendrehanlage**

ments. For a detailed description of the set-up and function see [6].

2.4 Receiving antenna FA 6

For determining a magnetic field accurately, the strength a n d direction of the magnetic vector must be known. The direction-finder antenna (FA 6) built especially for this purpose is intended for determining the direction of maximum field strength in space and the plane of minimum field strength that is perpendicular to this vector.

These conditions are fulfilled by the antenna shown in Fig. 2.5, similarly to the antenna FA 5 on gimbals described in [3].

The high sensitivity and Q factor of the antenna made a structure of synthetic material necessary for the direction-finder head. For this purpose, plexiglass was suited, hard PVC was chosen for the screws. Commercial 360-degree protractors with a reading accuracy of 30' were used for the angular scales. All angles were read by means of double-line plexiglass disks without parallax error.

For the angles of $\alpha$ and $\beta$ (planes A and C), the position $0^\circ$ can be chosen arbitrarily with a ring that can be adjusted with respect to the turntables A and C. The angles are read by means of the plexiglass rings fixed by a plastic screw. For the purpose of measurement, plane A of angle $\alpha$ is adjusted horizontally on the tripod by means of a built-in spirit level, plane B($\beta$) being oriented toward north by means of an accurate compass. The setting ring of plane A is then set to $\alpha = 0^\circ$ where it is fixed. If the antenna rod in plane C (angle $\varphi$) is adjusted such that it lies in plane B($\beta$), the direction-finder rod can be rotated into any direction through $\alpha$ and $\beta$, and the maximum field strength can then be determined (two degrees of freedom are sufficient for describing a general rotation). The minimum plane vertical to it is then adjusted by turning angle $\beta$ through $90^\circ$. A variation of $\varphi$ describes the minimum plane.

When turning the direction-finder head through angle $\beta$, it

would tip over together with the ferrite rod which might knock against the tripod. This possibility is eliminated by means of a return spring (bronze) built into the rotating mechanism which by its progressive action compensates the tipping moment of the ferrite rod in any position. The actual antenna is a slit ferrite rod, length 400 mm and diameter 13 mm, made of ferrite material 550 N 25 by Siemens & Halske. If the rod winding is connected asymmetrically with the impedance transformer without a transformer being connected between them, the voltage of the electrical dipole adds to the induction voltage caused by the magnetic field. This would cause incorrect voltage values and angular deflections, especially in the direction of minimum magnetic induction. The symmetrization necessary for accurate measurements was attained by providing the winding of the antenna rod with a symmetrical output and central grounding (cf. Fig. 2.6) in accordance with the report of [7]. The results were very good, the sensitivity to touch being negligibly small.

The antenna circuit is tuned at the secondary side of the transformer. The input signal is fed into the selective transmission measuring set (Type SPM-2, Wandel & Goltermann) via an impedance transformer and preamplifier (with four ranges from 0 to 60 dB). The circuit diagram of the impedance transformer and preamplifier is shown in Fig. 2.6.

The receiver is calibrated in $Wb/m^2$ by a method described in detail in [4]: The ferrite antenna is put into the field of a calibration coil accurately defined by Biot-Savart's law and the induced voltage is measured. From a suitable series of measurements for the frequency of interest (120 kc/sec), the calibration factor is calculated by least squares adjustment:

$$c = 6.5 \cdot 10^{-13}\ Wbm^{-2}/mv \pm 7.5\% \text{ (at 40 dB preamplification)}.$$

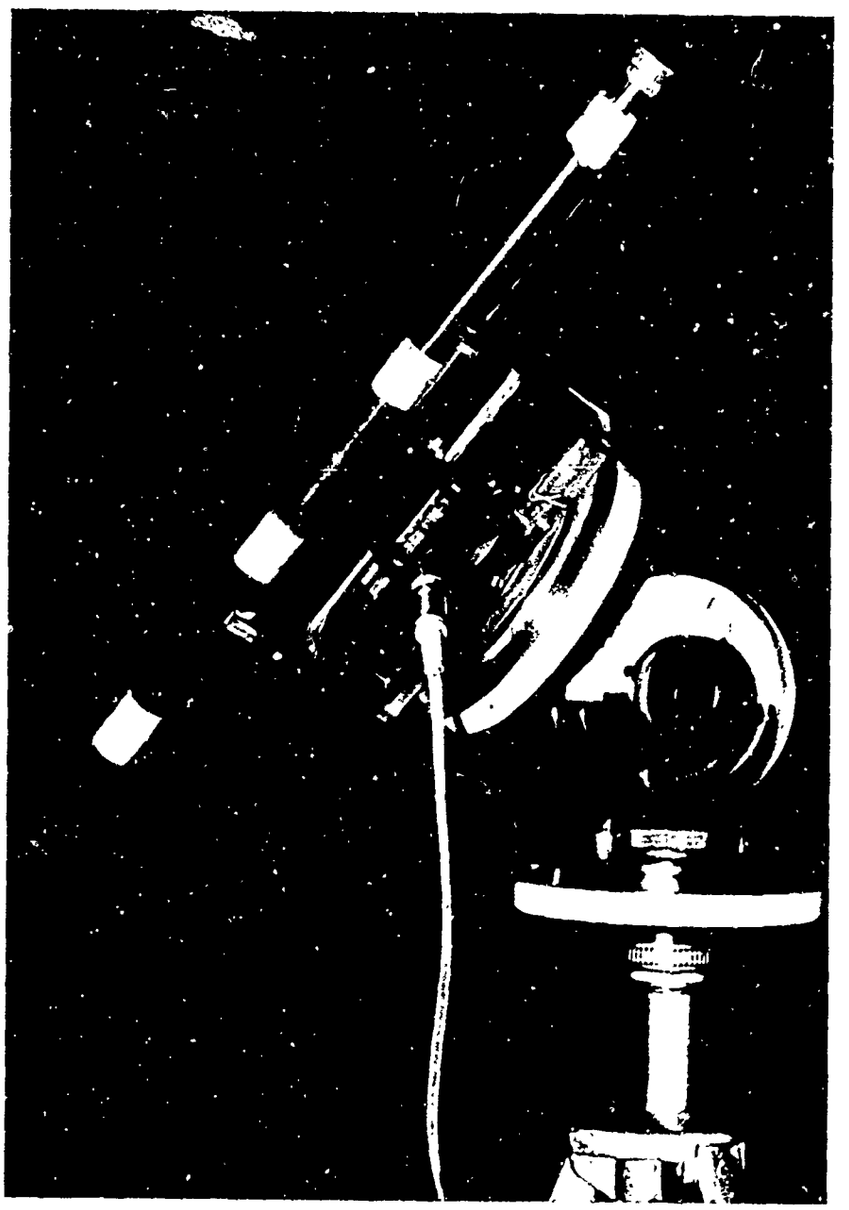

Fig. III

Receiving antenna FA 6 (ferrite rod) on the plexiglass bearing head rotatable on gimbals. Foreground: screened cables for connecting the antenna with preamplifier and tuning unit.

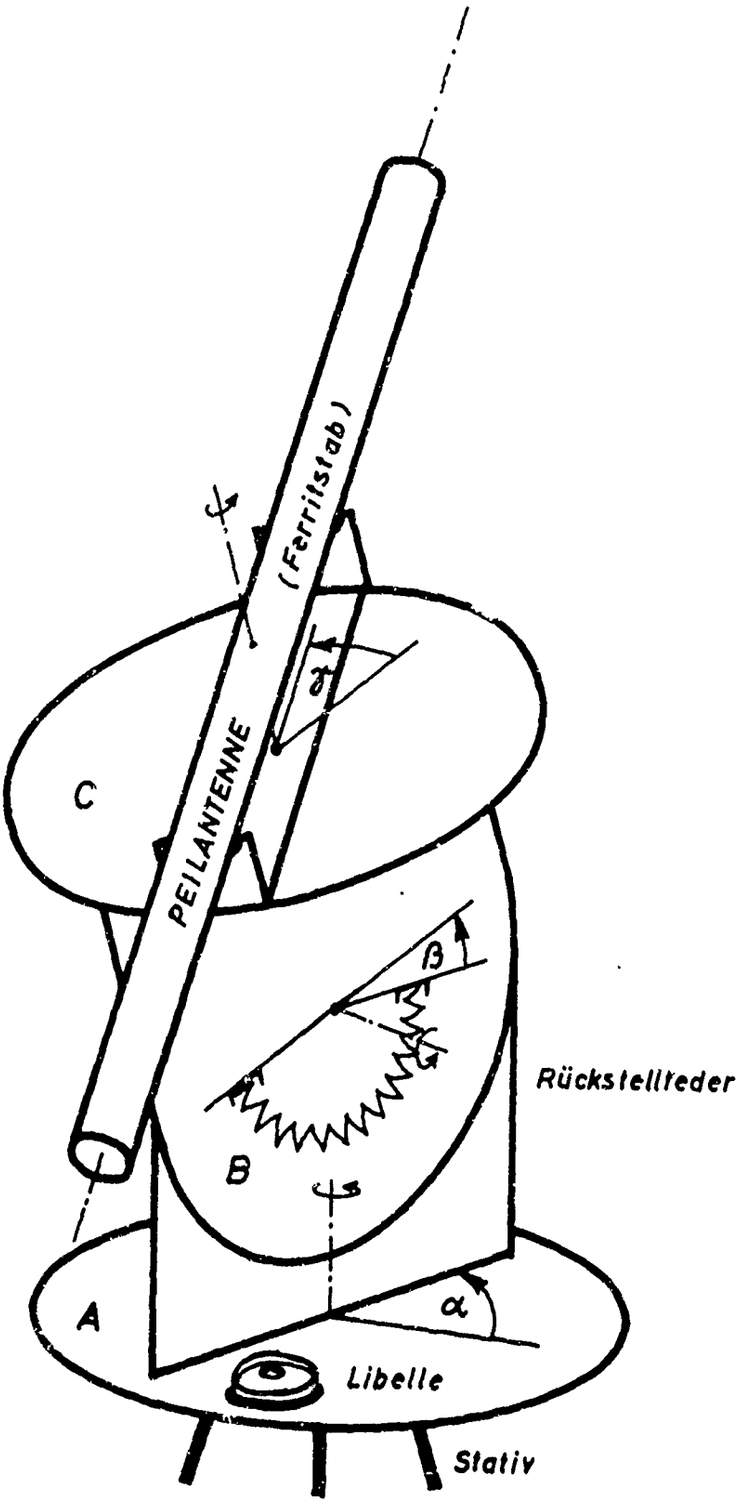


Peilkopf (schematisch)

Empfangsantenne FA6

Fig.: 2.5

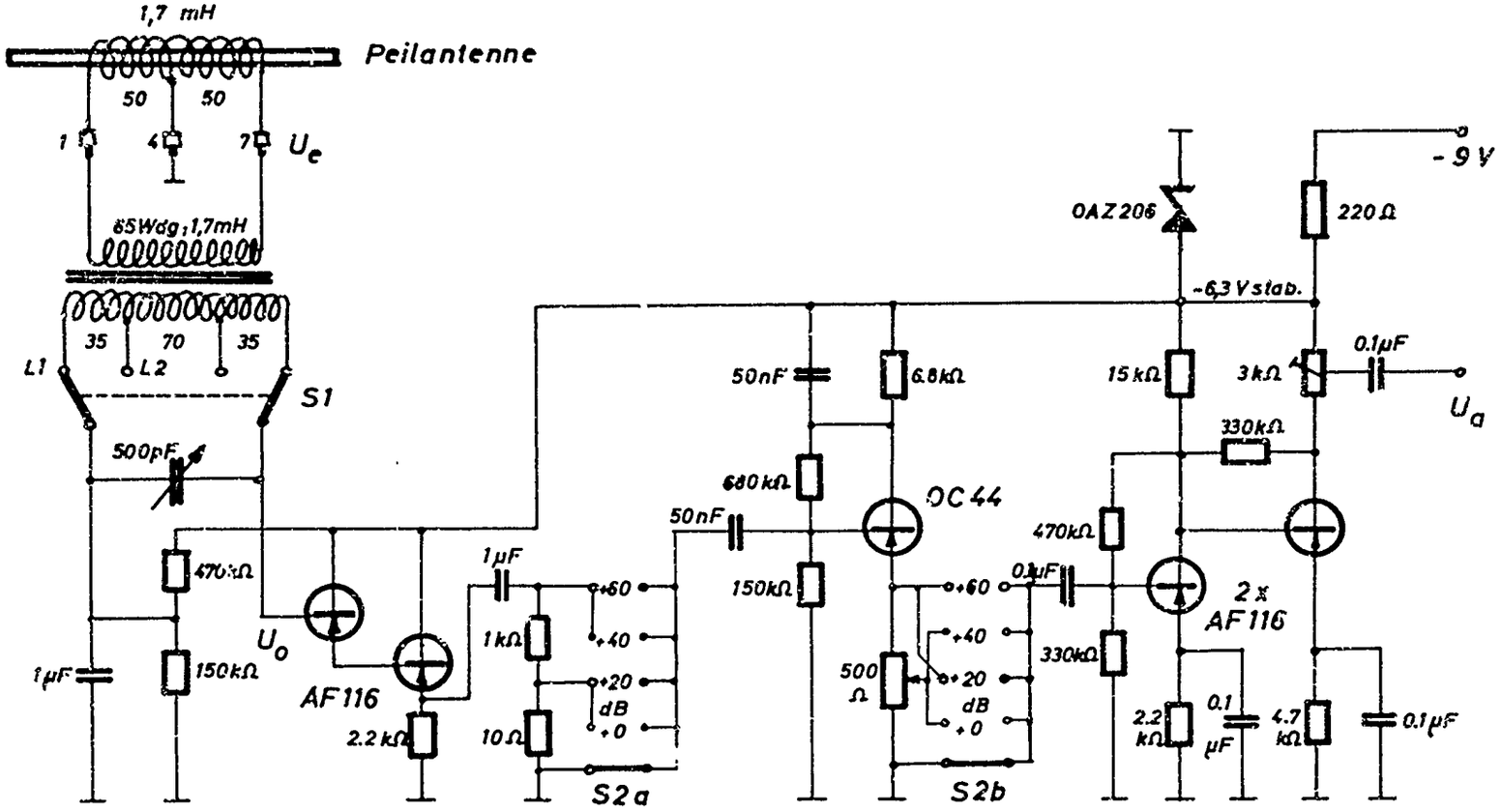


*Empfänger*

*FA 6 + 60 dB-Verstärker*

*Fig.: 2.6*

For comparing the experimental results (voltage values) with the field strength values calculated according to Chapter 1, the induction B at the point of measurement is computed from experiment and theory.

The experimental results are to be multiplied by the calibration factor c:

$$B_{exp}\left[\mathrm{Wb/m^2}\right] = c\left[\mathrm{Wbm^{-2}/mv}\right] \cdot U_{ind}\left[\mathrm{mv}\right] \qquad (13)$$

The theoretical values ($h_r$, $h_\perp \rightarrow h_{th}$) are multiplied by the transmitting dipole strength m and the scale constant $\mu_o$:

$$B_{th}\left[\mathrm{Wb/m^2}\right] = m\left[\mathrm{am^2}\right] \cdot \mu_o\left[\mathrm{vs/am}\right] \cdot h\left[\mathrm{m^{-3}}\right] \quad . \qquad (14)$$

For a simple comparison between experiment and theory it is often desirous to check the consistency of the values by families of curves. $B_{th}$ contains the strength m of the transmitting dipole which may vary from one experiment to another. Therefore, the tabulation and graphical representation of $B_{th}$ is very special.

This specialization can be avoided by comparing the "reduced" field strength h instead of the induction B. Hence we have

$$h_{exp} = \frac{B_{exp}}{m\mu_o} = \frac{c \cdot U_{ind}}{m \cdot \mu_o} \quad \left[\frac{\mathrm{Wbm^{-2}/mv \cdot mv}}{\mathrm{am^2 \cdot vs/am}} = \frac{1}{\mathrm{m^3}}\right] \qquad (15)$$

where all variable quantities of the experiment are contained in $h_{exp}$, $h_{th}$ being dependent only on the given frequency and the material constants. The experimental results are thus converted as to their quantity and dimensions so that they can be directly compared with the theoretical values graphically shown in various forms in Chapter 1.

2.5 Theory of measurements with the direction-finder antenna

As to the results of measurement described in Chap. 3 it must be mentioned that the transmitting antenna emits waves whose polarization is not always purely linear. The emitted wave may be polarized elliptically, since the propagation takes place partly in the form of a conduction current, and partly in the form of displacement current [8] . In this case, the wave arriving at the point of reception cannot be described by one vector only; for a more accurate description, the direction of the elliptical plane (direction of the normal) and the directions and values of the two elliptical axes are required.

These three quantities which are orthogonal to each other, are represented by three voltages, $U_1$, $U_2$ and $U_3$, which are induced in the rod at the corresponding position of the ferrite antenna.

The voltage $U_{ind}$ induced in the ferrite rod represents the projection of the diameter of the rotating field ellipse yielding the largest absolute value of $U_{ind}$ [8] . Fig. 2.9a shows that this need not be the diameter lying in the direction of the ferrite rod. The dashed curve gives the actual voltage $U_\mu$ for every angle of $\mu$ (for $U_2 = 0$, this will be exactly the cosine dependence).

If the ferrite rod does not lie in the plane of the rotating field ellipse, $U_{ind}$ is obtained by a plane which is perpendicular to the ferrite rod and which touches the ellipse. The latter is thus replaced by a three-axial ellipsoid whose third axis is formed by $U_3 \neq 0$. The schematic diagram of Fig. 2.9b indicates the enveloping surface resulting from it. From the mathematical viewpoint this is an elliptical toroid whose diameter oscillates when rotating.

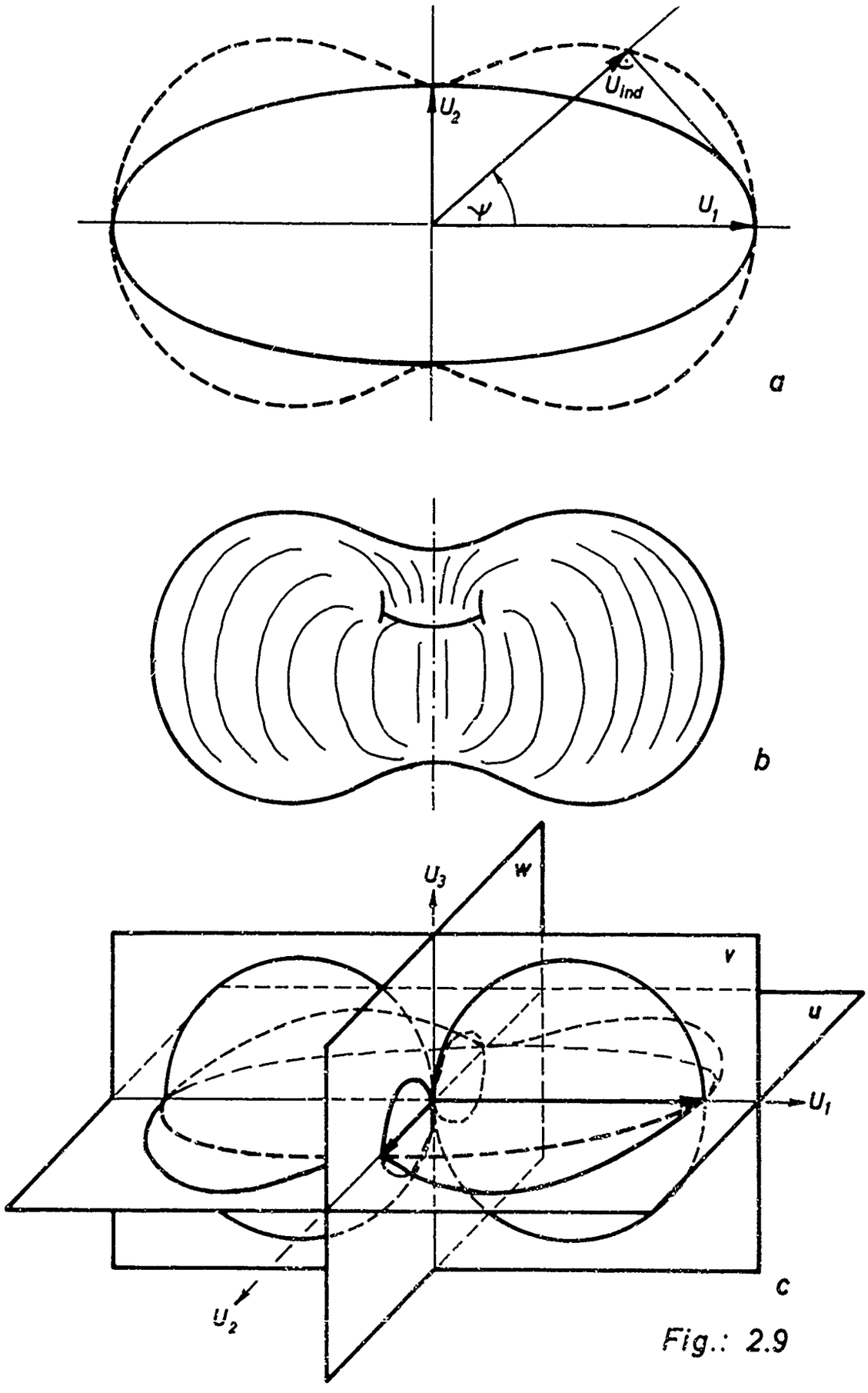


Fig.: 2.9

For a rotation of the ferrite rod in any plane it can be shown (cf. Fig. 2.9c) that the smallest induced voltage always lies in the plane perpendicular to $U_1$ (plane w).

For the purpose of measuring the above-mentioned characteristics of the rotating-field ellipse which actually may have any inclined position, the direction-finder antenna FA6 can be adjusted by two different methods.

Method I:

1. Original position: plane A horizontal, plane B directed toward north $\Rightarrow \alpha = 0^\circ$, $\varphi = 0^\circ$; ferrite rod lying in plane B (cf. Fig. 2.5).
2. $\beta = 0^\circ$, $\varphi = 90^\circ$, change $\alpha$ until $U_{ind} = \min$; fix $\underline{\alpha}$.
3. $\varphi = 0^\circ$ change $\beta$ until $U_{ind} = \min$; fix $\underline{\beta}$.
4. Change $\varphi$ until $U_{ind} = \min \Longrightarrow \underline{U_3}$ $\varphi$

   the resulting angles $\alpha$, $\beta$ and $\varphi$ are then recorded.
5. $\varphi \pm 90^\circ$, $U_{ind} \Rightarrow \underline{U_2}$
6. $\varphi = 0^\circ$, $\beta \pm 90^\circ$, $U_{ind} \Rightarrow \underline{U_1}$.

The six quantities $\alpha$, $\beta$, $\varphi$, $U_1$, $U_2$ and $U_3$ are uniquely adjusted in five steps. For the accurate adjustment of $U_3$ the angles $\alpha$ or $\beta$ can be corrected after step 4. The minimum voltage $U_3$ should be small as compared to $U_1$, thus being a measure of the accuracy of the angle measurement.

After step 4, plane C of the bearing head (cf. Fig. 2.5) lies in the direction of minimum induction, i.e., perpendicular to $U_1$. It thus contains $U_2$ and $U_3$ (cf. Fig. 2.9c, plane w). With $\varphi = 90^\circ$, the minimum voltage in the horizontal plane A (step 2) is adjusted so that the maximum ($\varphi = 0^\circ$) falls into plane B, its direction being given by angle $\alpha$. In most measurements, $U_1$ was approximately horizontal, $\alpha$ being identical with $\Psi_N$ (angle of the field strength $\vec{H}$ facing north; $\vec{H}$ is represented by $U_1$ with sufficient accuracy).

Method II:

1. Original position the same as in method I.
2. $\varphi = 0^\circ$, $\alpha$ and $\beta$ to be varied simultaneously until $U_{ind}$ = absolute minimum $\Rightarrow U_3$; fix $\underline{\alpha}$, $\underline{\beta}$.
3. $\beta \pm 90^\circ$, change $\varphi$ until $U_{ind}$ = min $\Rightarrow \underline{U_2}$.
4. $\varphi \pm 90^\circ$, $U_{ind} \Rightarrow \underline{U_1}$.

In this method, $U_3$ is adjusted asymptotically. In the most unfavorable cases, this requires a multitude of steps. After step 2, the ferrite rod has the normal direction of the elliptical plane ($U_3$). After step 3, the plane C is identical with the elliptical plane u ($U_1$, $U_2$), cf. Fig. 2.9c, which in some cases yielded illustrative experimental results. The theoretical evaluation, however, is much more difficult than in method I, since the angle $\Psi_N$ must be calculated from the combination of $\alpha$, $\beta$ and $\varphi$. It was owing to this drawback as well as to the difficult asymptotic adjustment of $U_3$ that method I which is less illustrative but easier to evaluate, was used almost exclusively for determining the ellipse and its parameters.

It was proved by experiment that method I and method II yield exactly the same voltage values of $U_1$, $U_2$ and $U_3$, thus yielding also the same angular positions. An analytical proof can be given by means of quaternions, but would be too small a detail to be included in the present report.

The orthogonal field strength components $\vec{H}_r$ and $\vec{H}_\varphi$ represented in the equations (1) and (3) are combined into one vector $\vec{H}$ if they are in phase. $\vec{H}$ then forms the diagonal of the rectangle formed by $\vec{H}_r$ and $\vec{H}_\varphi$ (cf. Fig. 1.2). If $\vec{H}_r$ and $\vec{H}_\varphi$ are not in phase, a rotating field ellipse results which analogously to the Lissajous figures is inscribed in the rectangle over $2 \cdot \vec{H}_r$ and $2 \cdot \vec{H}_\varphi$ (cf. Fig. 2.10). A detailed study of the polarization effects shall be the subject of a separate report.

In the present report, it will be estimated how far the neglection of the phase shift still lies within the accuracy of

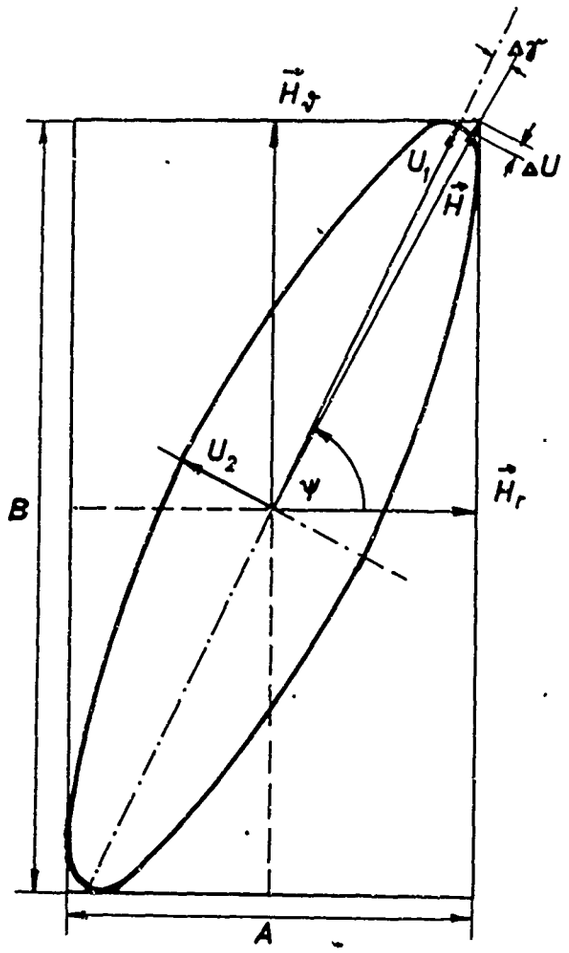


*Fig.: 2.10*

measurement.

A rotating field ellipse on principle forms only if two non-parallel components are added which are out of phase. Hence an elliptical polarization cannot exist at $\varphi = 0^\circ$ and $\varphi = 90^\circ$ where only the components $\vec{H}_r$ and $\vec{H}_l$ occur. Thus, the consideration of $U_1$ alone yields a complete evaluation. The quotient $G = H_0/H_{90}$ is therefore independent of a possible phase shift.

For values of $\varphi$ lying between 0 and 90°, $\vec{H}$ consists of the two components $\vec{H}_r$ and $\vec{H}_l$. The ratio

$$\frac{A}{B} = \frac{|\vec{H}_r|}{|\vec{H}_l|} = G \cdot \cot\varphi \qquad (16)$$

is decisive for determining the error. A/B determines the axial ratio of the rectangle, in which the rotating-field ellipse is inscribed. The axial ratio $U_2/U_1$ of the ellipse is a measure of the phase shift between $\vec{H}_r$ and $\vec{H}_l$. If the experimental value of $U_1$ is compared with the theoretical $\vec{H}$, we obtain an amplitude error of

$$\Delta U = 100\ (1 - \frac{U_1}{|\vec{H}|})\% \qquad (17)$$

and an angular error of $\Delta\varphi$ (angle between $\vec{H}$ and $U_1$).

The table gives the error to be expected for some combinations of A/B and $U_2/U_1$.

TABLE OF ERRORS

| $U_2/U_1 \rightarrow$ | 0.1 | | 0.2 | | 0.3 | | 0.5 | |
|---|---|---|---|---|---|---|---|---|
| A/B ↓ | $\Delta\varphi$ | $\Delta U$ | $\Delta\varphi$ | $\Delta U$ | $\Delta\varphi$ | $\Delta U$ | $\Delta\varphi$ | $\Delta U$ |
| 3 | 1.5° | 1% | 4° | 2% | 18° | 6% | - | - |
| 2 | 1° | 0.6% | 2° | 2% | 6° | 5.5% | 26° | 12% |
| 1.5 | 0.7° | 0.7% | 1.5° | 3% | 4° | 6.5% | 9° | 10.5% |
| 1.25 | 0.3° | 1% | 1° | 3.5% | 2° | 7.5% | 4.5° | 11.5% |
| 1.0 | 0° | 2% | 0° | 4% | 0° | 7.7% | 0° | 12.3% |

The derivation of the necessary equations is elementary but complicated, therefore only the results are given herein.

An illustrative, but less accurately evaluable picture of these relations is obtained by representing the Lissajous figures on the oscilloscope and by varying the phase position.

From the table it can be seen that the error will be negligibly small for an ellipse with the axial ratio $U_2/U_1$ being less than 0.2. For $U_2/U_1 = 0.3$, the amplitude error still lies within the accuracy of measurement, whereas the error of angle in an accurate measurement would have to be taken into account. For the case of $U_2/U_1 = 0.5$ which in the described measurements occurs only rarely, the amplitude error is larger than the expected accuracy of measurement. As the experience of measurements showed it is not meaningful to evaluate deviations that lie below 15%, since the homogeneity of rock is insufficient.

For judging the angular deflection it must be taken into account that $U_2/U_1 \sim 0.5$ occurred in measurements where G was near unity and $\vartheta$ was about $45^\circ$. Here too, the angular deflection is negligibly small.

The result of this examination shows that the approximation of

$$U_1 \sim \vec{H}$$

is admissible for the used method of evaluation.

## 3. Directivity pattern measurements with the portable transmitter

Most of the experimental measurements were made in the mine of Großkogel near St. Gertraudi/Tyrol. The miner's map of Fig. 3.1 shows the air-conditioned laboratory with the above-mentioned transmitter for the stationary unit, and the electronic measuring site.

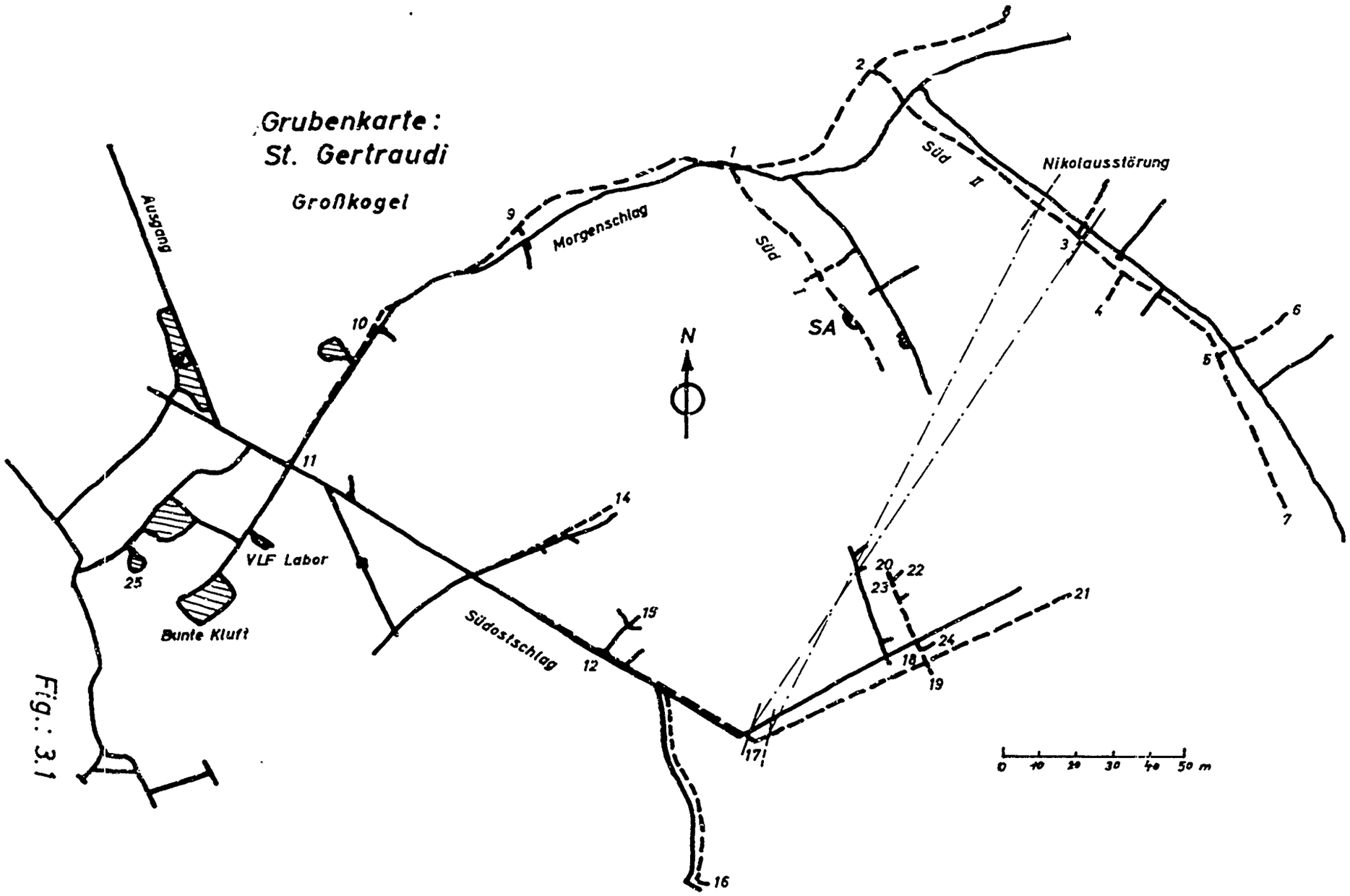
Grubenkarte:
St. Gertraudi
Großkogel
Ausgang
Morgenschlag
Süd I
Süd II
Nikolausstörung
SA
N
VLF Labor
Bunte Kluft
Südostschlag
1
2
3
4
5
6
7
9
10
11
12
14
15
16
17
18
19
20
21
22
23
24
25
0 10 20 30 40 50 m

Fig.: 3.1

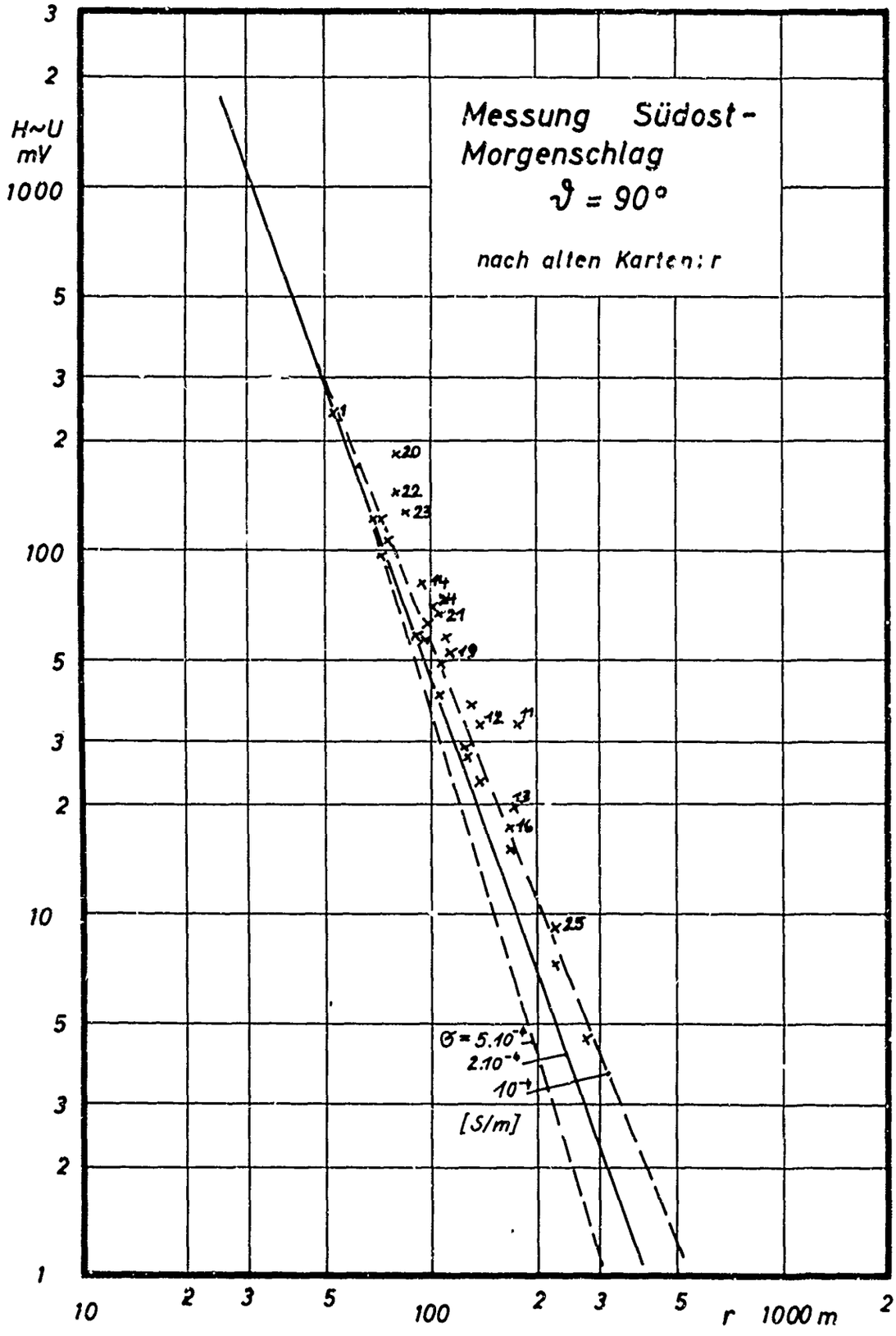
Messung Südost-
Morgenschlag
ϑ = 90°
nach alten Karten: r
H~U
mV
1000
100
10
r 1000 m
σ = 5.10⁻⁴
2.10⁻⁴
10⁻⁴
[S/m]

Fig.: 3.2

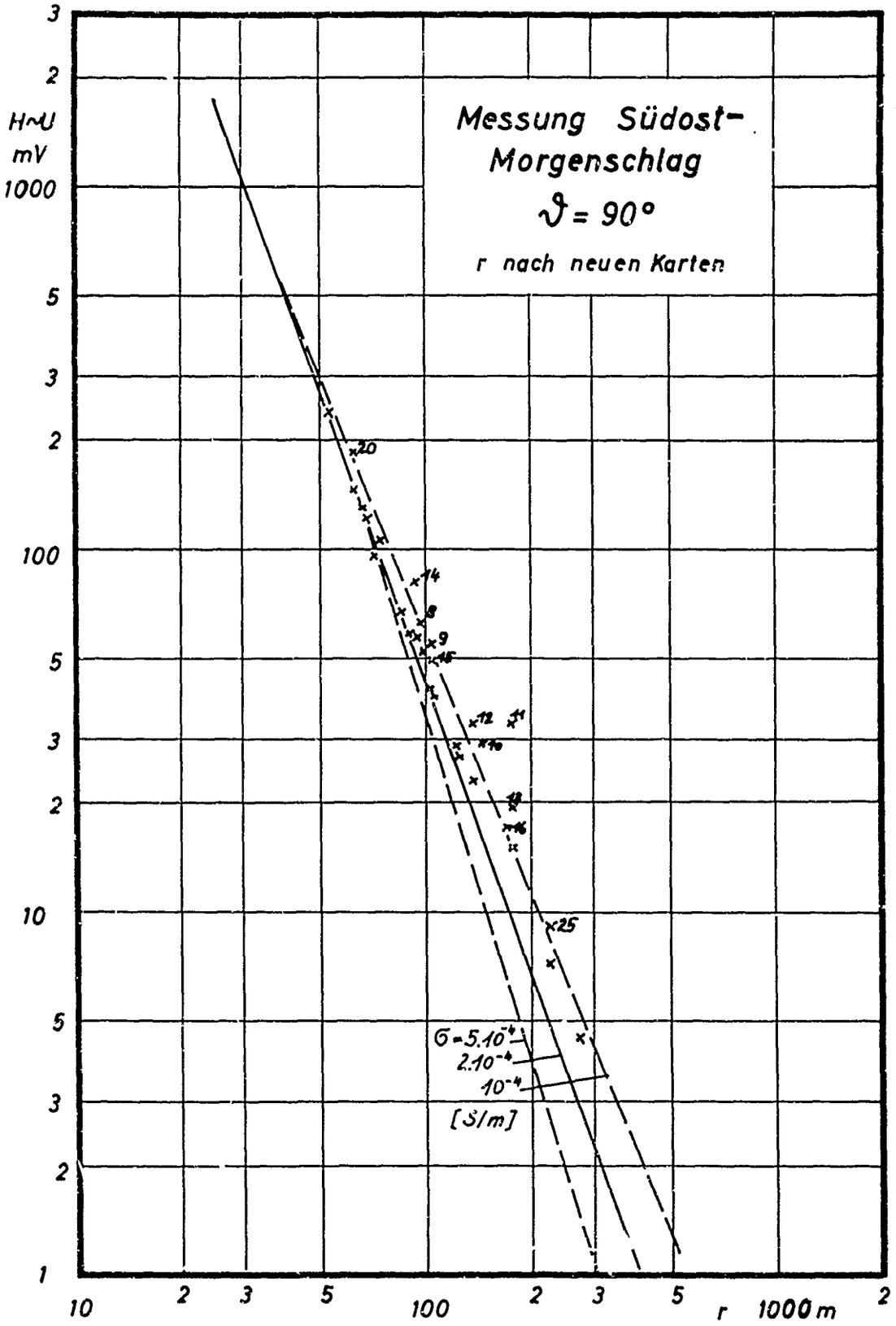
Messung Südost-
Morgenschlag
ϑ = 90°
r nach neuen Karten
H~U
mV
1000
100
10
σ = 5.10⁻⁴
2.10⁻⁴
10⁻⁴
[S/m]
r 1000 m

Fig.: 3.3

Usually it is impossible to make measurements righ round the transmitting antenna in the mine, therefore the antenna is being rotated, without changing the location of transmitter and receiver. Furthermore, a measurement of angle between transmitter and receiver is impossible; therefore, all angles are at first related to the northern direction by means of a geological compass (Breithaupt, Kassel) (cf. Fig. 3.4). Thus, the angles $\vartheta_N$ (transmitting antenna) and $\alpha$ (receiving antenna) are obtained. Then the angle of the line connecting transmitter and the point of measurement is measured on the miner's map ($\varphi_N$). The angles $\vartheta$ and $\psi$ (cf. Fig. 1.1) in the theoretical expressions yield the following relations:

$$\begin{aligned} \vartheta &= \vartheta_N - \varphi_N \\ \psi &= \varphi_N - \alpha \ . \end{aligned} \tag{18}$$

For the purpose of a simple and illustrative comparison with the angles obtained theoretically, $\vartheta$ and $\psi$ are defined as follows:

$$\begin{aligned} &-90^\circ < \vartheta \leq +90^\circ, \quad \text{else } \vartheta' = \vartheta \pm 180^\circ \\ \text{and} \quad &-90^\circ < \psi \leq +90^\circ, \quad \text{else } \psi' = \psi \pm 180^\circ. \end{aligned} \tag{19}$$

The physical reason for this definition is the fact that the voltage values of transmitting antenna and receiving antenna on rotation about $180^\circ$ are exactly the same, a fact which theoretically is understood ad hoc and which has been proved by experiment. The symmetry of the ferrite rod receiving antenna was attained by a set-up which is perfectly symmetrical from a mechanical and electrical viewpoint.

From the multitude of measurements which are in good agreement with the above theory, let us discuss only one very typical case.

A. Standard measurement Südostschlag:

The range of measurement stretches from the end of Südostschlag (SA) MP 21 (cf. miner's map 3.1) to the bend Südostschlag (DA) MP 17 length 92 m, direction toward north $\varphi_N = 242^\circ$. The angles of

$\vartheta$ and $\psi$ are calculated from equation (18). G = 1.4 with good approximation is the ratio of $H(\vartheta = -2^{\circ})$ : $H(\vartheta = 68^{\circ})$, i.e., the ratio of the corresponding voltage values. The angles $\psi_t$ for comparison with experiment are the field directions which are to be expected from (12) with G = 1.4. They are in good agreement with experiment. Fig. 3.5a shows the directivity pattern of the transmitting antenna and receiving antenna. The tabulated values of the above and all other measurements are recorded in [6].

As the directivity pattern is plotted for a stationary transmitting antenna, the angle $\psi$ had to be plotted clockwise, i.e., in opposite sense to $\vartheta$ for reasons of analogy. The angle $\vartheta$ (cf. Fig. 3.4) is counted positively from the axis of the transmitting antenna to the radius vector, whereas $\psi$ although counted clockwise and positive, is counted from the radius vector to the receiving antenna axis.

B. Profile measurement Westschlag:

A number of directivity patterns were measured at approximately equidistant points along the Westschlag (an almost straight gallery through largely dead rock connecting the Großkogel with the Kleinkogel mine). They are plotted as directivity patterns of the receiving antenna in Fig. 3.6 in the same scale on the map. Hence the changes in main lobe direction can be recognized in good agreement with the diagram of Fig. 1.6: at the points 1 and 2, the large axis of the "receiving ellipse" points toward the transmitter, whereas the diagram in 3 is about circular; from 4 onward, the principal axis is vertical to the radius vector. From thereon we would have to speak in terms of the far field (cf. Chapter 1).

The conductivity of $2 \cdot 10^{-4}$ mhos/m thus determined for this region is in good agreement with the statements of [9] and [10].

If the directivity pattern of transmitting and receiving antenna is considered as being stationary and if the symmetry axis of the diagrams is identified with the ray direction of a wave

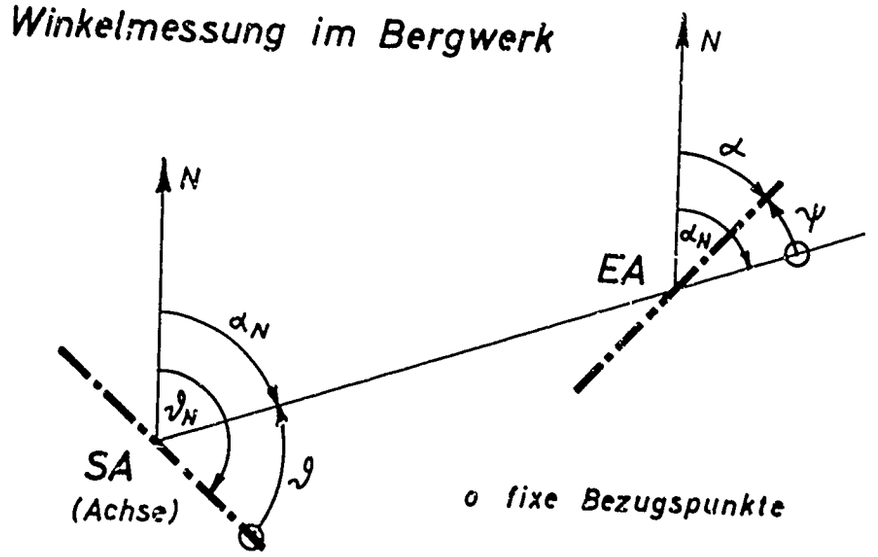
Winkelmessung im Bergwerk
N
N
EA
SA
(Achse)
o fixe Bezugspunkte

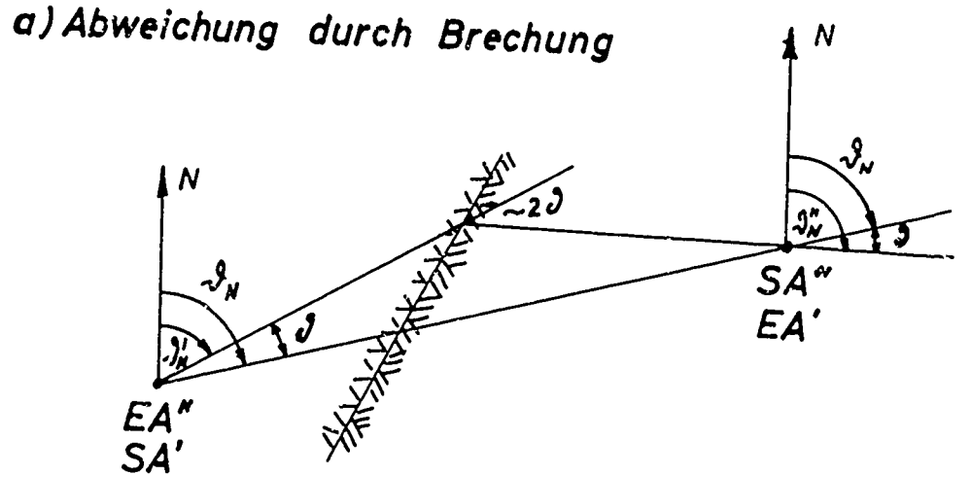
a) Abweichung durch Brechung
N
N
SA''
EA'
EA''
SA'

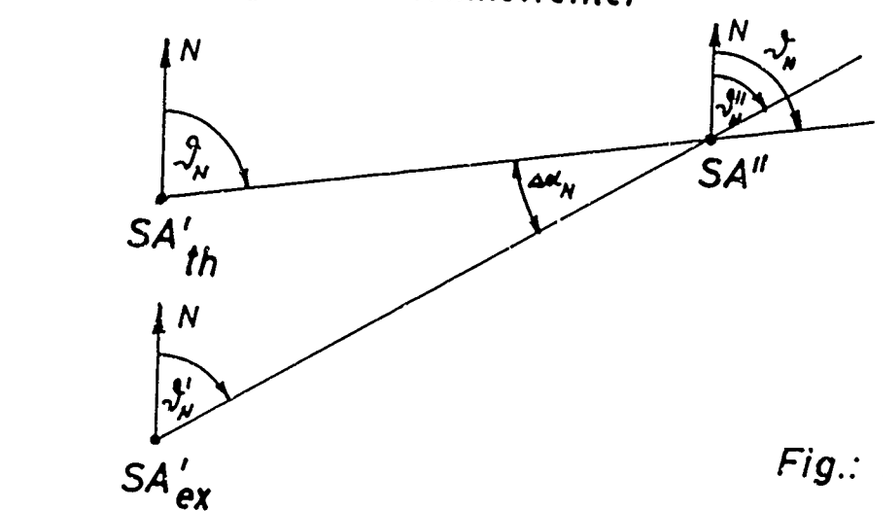
b) Abweichung durch Winkelfehler
N
N
N
SA''
SA'th
SA'ex

Fig.: 3.4

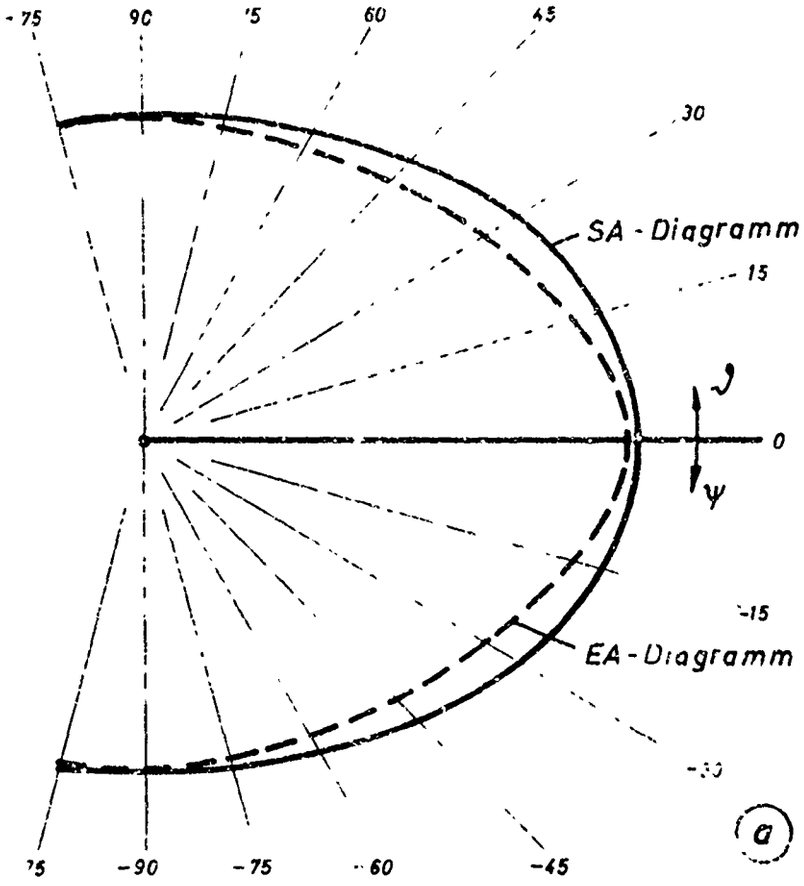


Normalmessung
Gertraudi

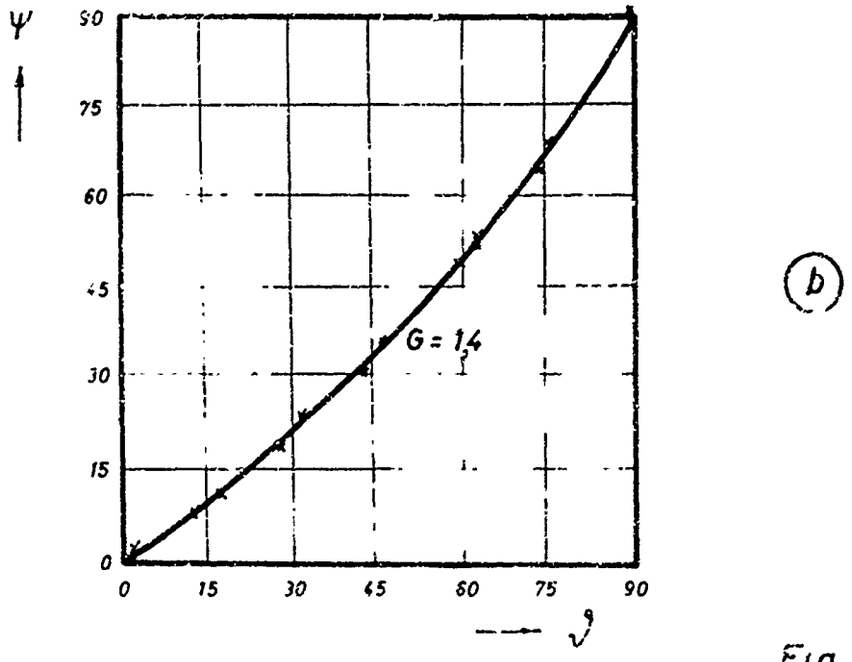


Fig : 3.5

**Profilmessung:**
**Westschlag**

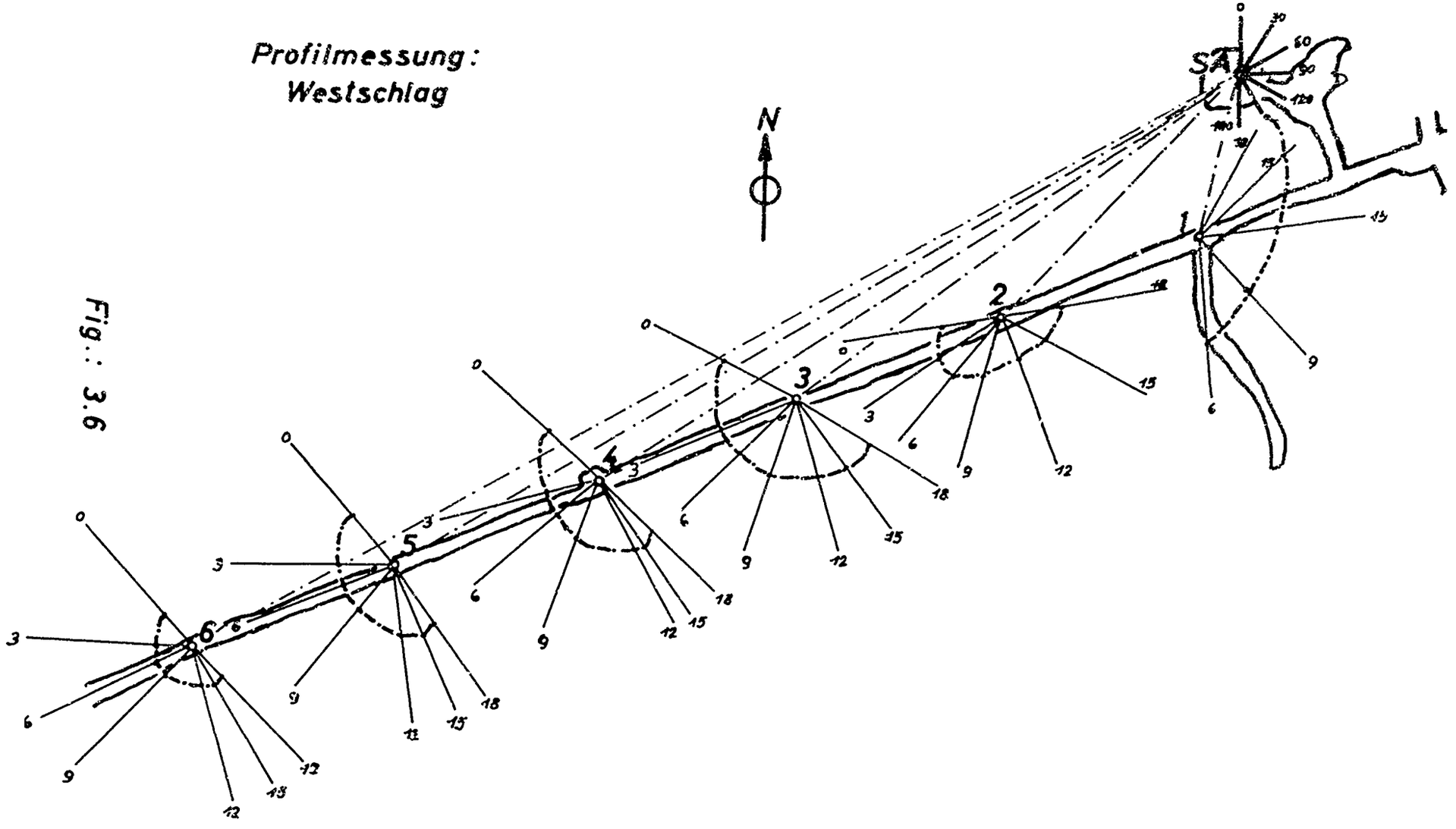


Fig.: 3.6

front for the purpose of obtaining connection of fields of high frequency (which according to the experimental results can be done in first approximation), considerations may be applied which are similar to those of geometrical optics.

It is owing to the method of evaluating the directivity patterns measured, that a disturbance lying between transmitter and receiver has a similar effect on all the results of measurements for various $\vartheta$ values.

If the equation

$$\Delta\psi = \psi - \psi_t \tag{20}$$

which has already been used above, is applied for calculating the angular deflections between the actually measured value of $\psi$ and the corresponding theoretical angle $\psi_t$, the resulting deviations $\Delta\psi$ are about the same for all $\vartheta$ values. Their mean value $\overline{\Delta\psi}$ is a measure of the deviation of the symmetry line of the diagram from the radius vector.

Hence it is impossible to make unique conclusions from the deviations of the angles in a directivity pattern to the deviation in the miner's map, or to a geological disturbance. It is, however, almost always possible to exchange transmitter and receiver for a second measurement (cf. Fig. 3.4a). For an approximate consideration ($\vartheta = 0^\circ$ ... symmetry axis in correspondence with the lobe direction, thus $\vartheta_N = \varphi_N$) we have the following relation

$$\begin{aligned} \vartheta'_N &= \vartheta_N - \delta \\ \vartheta''_N &= \vartheta_N + \delta \end{aligned} \tag{21}$$

for

a) a geological disturbance in the form of an interface between a zone of low conductivity and one of higher conductivity. $\vartheta_N$ is the undisturbed direction, $\vartheta'_N$ is the apparent refracted direction from transmitter to receiver, $\vartheta''_N$ holds for an exchange of transmitter and receiver.

For the two series of forward and backward measurements, the resulting $\Delta\Psi$ are approximately equal, having only opposite signs. This indicates a geological disturbance, i.e., a refraction. Furthermore we have

$$\text{sign}\,\overline{\Delta\Psi}_{\text{forw.}} = -\text{sign}\,\overline{\Delta\Psi}_{\text{backw.}} \qquad (22)$$

$\longrightarrow$ refraction

for the case of

b) a deviation owing to inaccurate miner's maps, compass errors or plane parallel refraction. Here, the following relation is valid (cf. Fig. 3.4b):

$$\begin{aligned} \vartheta'_N &= \vartheta_N - \varrho_N \\ \vartheta''_N &= \vartheta_N - \varrho_N \end{aligned} \qquad (23)$$

where $\vartheta_N$ is the direction taken from the map, $\vartheta'_N$ is the direction of the line connecting transmitter and receiver determined from the measured result, $\vartheta''_N$ holds for an exchange between transmitter and receiver. For the direction $\varrho_N$ determined from the miner's map, a correction must be made (suitably denoted with $\Delta\varrho_N$) which is to be calculated from the $\Delta\psi$ values, becoming either positive or negative for both series of measurement. Since the deviation $\Delta\varrho_N$ affects $\vartheta$ and $\Psi$ with opposite signs (cf. Eq. (18)) and $\Psi_t$ and $\vartheta$ are connected directly according to Eq. (12), we have

$$\overline{\Delta\Psi} \doteq 2\Delta\varrho_N \qquad (24)$$

(exact only for $G = 1$).

Hence follows

$$\text{sign}\,\overline{\Delta\Psi}_{\text{forw.}} = \text{sign}\,\overline{\Delta\Psi}_{\text{backw.}} \qquad (25)$$

$\longrightarrow$ map error or parallel displacement.

If the corrections are equal for both cases, a refraction caused by a geological disturbance is proved for one case, in the second case an inaccurate miner's map or a compass error or plane parallel displacement are responsible. If the two corrections are different, a coupled refraction can be distinguished from a parallel displacement and angular deflection by finding the difference between the two corrections within the accuracy of measurement.

c) Directivity pattern Südostschlag-Morgenschlag

In continuation of previous measurements which indicated an error in the map a number of directivity patterns were measured and evaluated with always 13 steps of $15^{\circ}$ in the region of Morgenschlag and Südostschlag. For a series of especially clear measurements with the corresponding backward measurement, the evaluation was made from the Eq. (20) - (25) and the diagrams were given in Fig. 3.7. The almost identical mean deviations $\overline{\Delta\varphi}$ both have a negative sign which according to the above theory and the results of previous measurements clearly indicates a map error. From Eq. (24) we obtain $\Delta\varphi_N = -8.2^{\circ}$. From the newly surveyed miner's map (Fig. 3.1) there results again an angular correction of $-8^{\circ}$.

The good agreement with theory shows the possibility of making a mine or gallery survey by means of VLF bearing. This is advantageous especially in those cases where the use of a theodolite involves considerable troubles. The accuracy of measurement increases as distance, conductivity and frequency decrease.

The highly interesting possibilities offered by this method of measurement led to a further development and generalization of the bearing method. A report shall be given at another occasion.

D. Measurement through ore in the mine of Lafatsch

The abandoned mine of Lafatsch offers highly suited sites of measurement, since the ore deposit (lead sulphide and zinc blende) has not been mined, furthermore the entire system of galleries is free of rails and tubes.

Several directivity patterns, the two most typical of which are shown, were measured across the ore blade hatched in Fig. 3.9. In this connection it must be mentioned that the measurement was not exactly backward, since there was not enough room for the antenna frame at site 386. For the backward measurement, the transmitting antenna had been set up at point 195 which lies approximately 13 m northwest of 386. This is the reason why the amplitudes of forward and backward measurements differed.

In one case the sum of $\Delta\Psi$ was found to be $37^{\circ}$, whereas for the backward measurement it was $-37.5^{\circ}$. This result which according to (22) indicates a refraction, is very clearly expressed in the diagram of Fig. 3.8. The angle of refraction can be taken from the representation according to Fig. 3.4, $\vartheta' \approx 20^{\circ}$.

This cloar effect of refraction offers some more possibilities: According to the actual geological conditions, the ore bed may be assumed to be a wedge whose refractive edge lies at the southern margin; its angle of refraction can be calculated from the equations of metal optics [11] (dissipative medium).

The following equation holds for the index of refraction of a conductive medium according to Joos [11] p. 312:

$$n = \sqrt{\frac{\mu}{2}\left(\sqrt{\varepsilon^2 + \mu_o^2 c^4 \delta^2/\omega^2} + \varepsilon\right)} \quad . \qquad (26)$$

Considering that the conductivity of dead rock for calculating the relative index of refraction $n_r = n_E/n_T$ is $\delta_T = 10^{-4}$ mhos/m, the wedge angle $\gamma$ for various values of $\delta_E$, ore conductivity, is calculated from the following table (anlge of refraction $\vartheta \approx 20^{\circ}$):

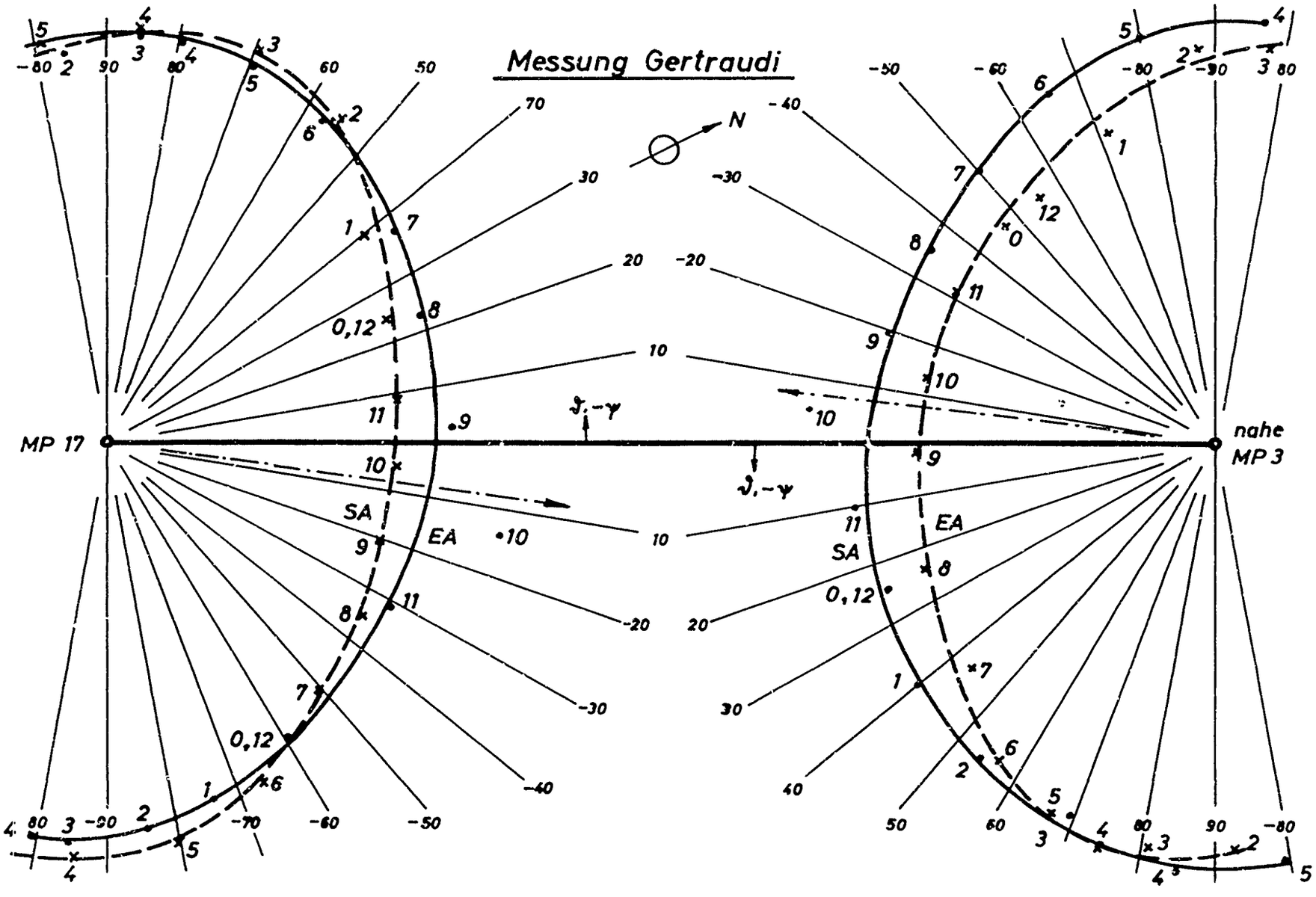


Fig.: 3.7

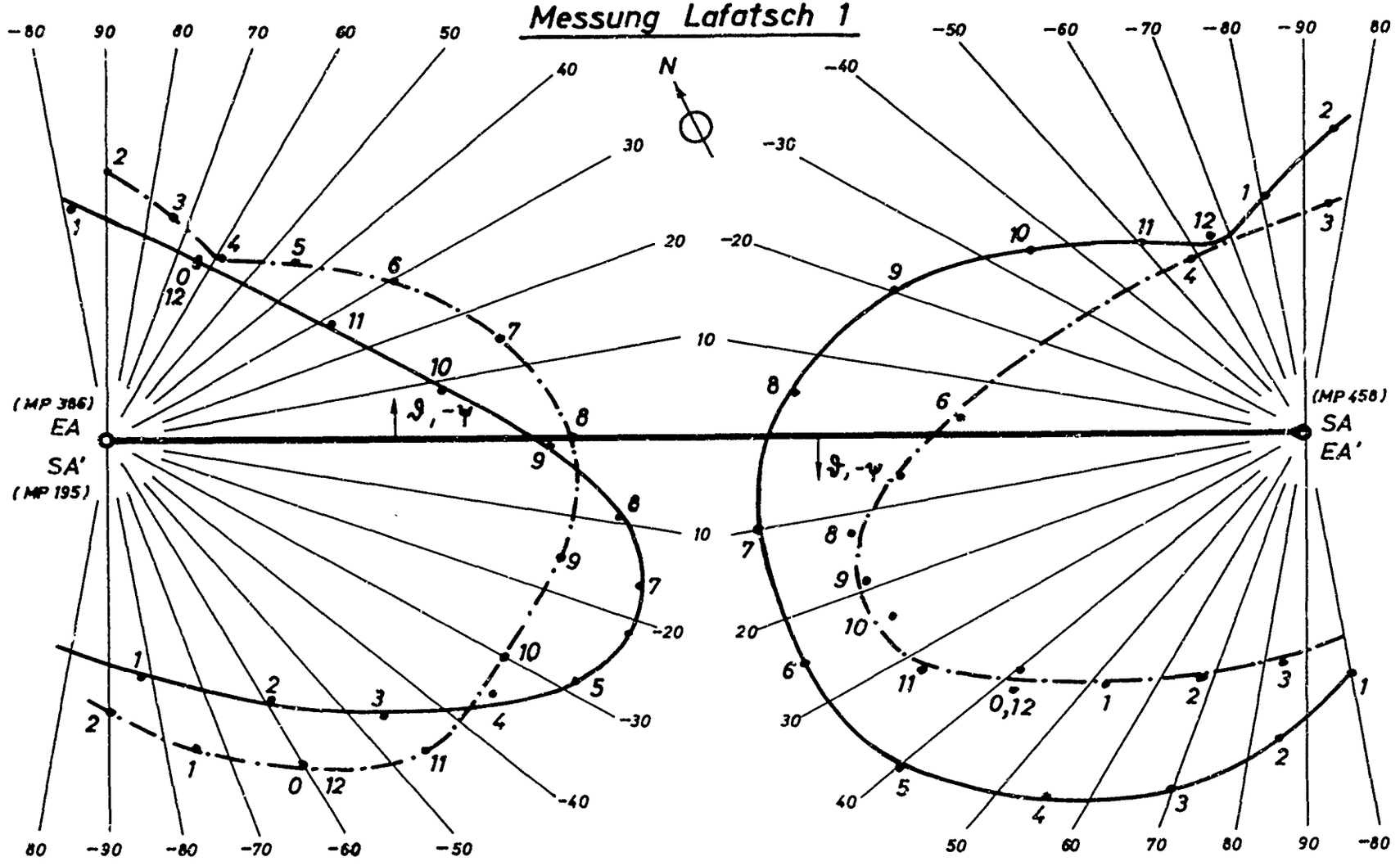


Fig. 3.8

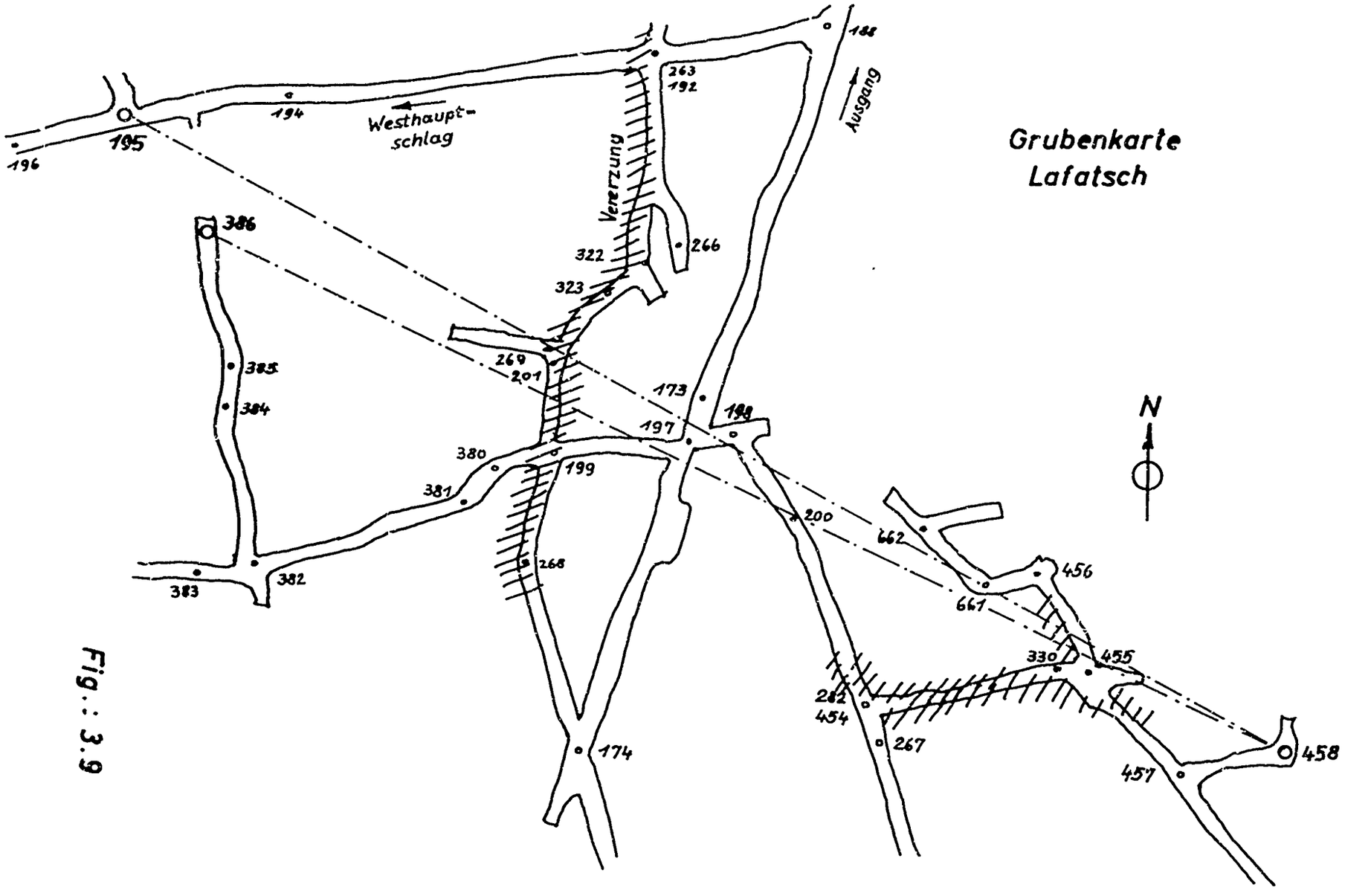
Grubenkarte
Lafatsch
Westhaupt-
schlag
Verzung
Ausgang
N
196
195
194
263
192
188
266
322
323
386
385
384
269
201
173
197
199
380
381
383
382
268
174
200
662
661
456
330
455
282
454
267
457
458

Fig.: 3.9

| $\sigma_E$ | $10^{-2}$ | $3 \cdot 10^{-3}$ | $10^{-3}$ mhos/m |
|---|---|---|---|
| $n_r$ | 7.0 | 4.0 | 2.2 |
| $\gamma$ | $6^\circ$ | $11^\circ$ | $21^\circ$ |

The conductivity $\sigma_E \leq 10^{-2}$ mhos/m determined in previous reports, yields a wedge angle of $6 - 8^\circ$ which might be in good agreement with the actual shape of the ore deposit.

Another possibility of checking this interpretation is offered by the deviation of the maximum from the horizontal. It is probable that the ore deposit is also a wedge lying in vertical direction so that the meridional plane (cf. Chapter 1) is "broken", thus causing the field direction to deviate from the plane; the measured deviations have the same order of magnitude as the values of $\Delta\psi$, which may be considered as a confirmation.

The great differences between individual $\Delta\psi$ values in Tables 7a and 7b require a detailed examination. The ratio of $U_2/U_1$ exceeds the value of 0.2 only in five of a total of 25 measurements. Chapter 2.5 (Table p. 15 ) shows that the amplitude and angular deflections for $U_2/U_1 = 0.2$ are negligibly small. The deviations $\Delta\psi$ which vary considerably therefore cannot be explained in this way by elliptical polarization.

Considering the symmetry line of the two diagrams in Fig. 3.8 as a zero line (as has been mentioned before), the angles $\vartheta$ and $\psi$ must also be calculated from this zero line.

The deviation taken from Fig. 3.8 is approximately $20^\circ$. For the forward measurement (SA at MP458, EA at MP366) the following relations are therefore valid for the corrected angles

$$\vartheta_k = \vartheta - 20^\circ, \qquad \psi_k = \psi + 20^\circ$$

and accordingly also

$$\vartheta_k = \vartheta - 20^\circ, \qquad \psi_k = \psi - 20^\circ$$

for the backward measurement.

The new deviations $\Delta\Psi_k$ thus calculated fluctuate much less about zero and have the order of the measuring error.

This is another proof of the fact that the directivity pattern may be considered as a whole, and that its symmetry line may be identified with the ray direction of a plane wave. It is even possible to make the evaluation in accordance with the laws of geometrical optics, if the coefficient of refraction for a conductive medium is determined as in metal optics.

Summary

From the results hitherto obtained we may conclude that the measurement of directivity patterns is a considerable progress in simplifying the evaluation. The formal analogy to geometrical optics is only one advantage; another step forward is the possibility of measuring the rock parameters directly on the solid rock, distinguishing especially between the different disturbing influences.

Besides the above-mentioned work on direction-finding methods by means of VLF waves, the examination of wave propagation at the rock-air interface is being prepared and has already been made in parts. A detailed report will be given after the completion of this work.

Furthermore, the near-field far-field transition is intended to be studied at still larger distances. The strong and portable transmitters and more sensitive receiving antennas necessary for this purpose are under construction.

## REFERENCES


[1] 1st Technical Annual Summary Report: On the propagation of VLF waves in solids, 61(052)-490, Dec. 1961

[2] 2nd Technical Annual Summary Report: On the propagation of VLF waves in solids, 61(052)-490, Dec. 1962

[3] 4th Technical Annual Summary Report: On the propagation of VLF waves in solids, 61(052)-490, Dec. 1963

[4] Final Scientific Report: On the propagation of VLF waves in solids, 61(052)-490, Dec. 1965

[5] Scientific Report Nr. 10: Magnetic dipole antennas for receivers by Dr. W. BITTERLICH, 61(052)-490, Sept. 1964

[6] N. NESSLER, Die Ausbreitung langer elektromagnetischer Wellen durch homogene und inhomogene feste Medien, Thesis, February 1967

[7] W. BITTERLICH, Magnetische Dipolantennen, Internationale elektronische Rundschau, Berlin 1967

[8] R AMBRONN, Methoden der angewandten Geophysik, Verlag Steinkopf, Dresden-Leipzig, 1926

[9] O. WÖRZ, Über die Dielektrizitätskonstante $\varepsilon$ und Leitfähigkeit $\sigma$ von Gestein, Thesis, May 1965

[10] O. GRÖBNER, Über die Ausbreitung sehr langer elektromagnetischer Wellen (VLF) Wellen im Gestein, Thesis, July 1964.

[11] G. JOOS, Lehrbuch der Theoret. Physik, Akademische Verlagsges. Leipzig, 1956.

DOCUMENT CONTROL DATA - R&D

1. ORIGINATING ACTIVITY (Corporate author)

Dr. Wolfram BITTERLICH Kaiser-Franz-Josefstr. 5
A-6020 Innsbruck, Austria

2a.

2b.

3. REPORT TITLE

PROPAGATION OF LONG ELECTROMAGNETIC WAVES THROUGH ROCK

4. DESCRIPTIVE NOTES (Type of report and inclusive dates)

SCIENTIFIC REPORT No. 2

5. AUTHOR(S) (Last name, First name, initial)

N. NESSLER

| 6. REPORT DATE | 7a. TOTAL NO. OF PAGES | 7b. NO. OF REFS |
|---|---|---|
| 15 April 1967 | 61 | 11 |

| 8a. CONTRACT OR GRANT NO. | 9a. ORIGINATOR'S REPORT NUMBER(S) |
|---|---|
| CONTRACT AF 61(052)-902 | |
| b. PROJECT AND TASK NO. 4600-11 | |
| c. ELEMENT 62405454 | 9b. OTHER REPORT NO(S) (Any other numbers that may be assigned this report) |
| d. SUBELEMENT 674600 | |

10. DISTRIBUTION STATEMENT

DISTRIBUTION OF THIS DOCUMENT IS UNLIMITED

11. SUPPLEMENTARY NOTES

12. SPONSORING ACTIVITY
United States Government
American Embassy, Brussels, Belgium

13. ABSTRACT

A description is given of the propagation of long electromagnetic waves through rock, in continuation of our previous studies on the VLF region. The theoretical bases of wave propagation are reviewed. Important results of comprehensive calculations are summarized and methods of measuring the propagation parameters $\varepsilon$, dielectric constant, and $\sigma$, conductivity, are derived. The instruments used for conducting the measurements are described. ~~Most of them had to be built by our team.~~

Measurements in the near field and in the near field - far field transition zone as well as through ore beds are evaluated.

( )

1

| KEY WORDS | LINK A | | LINK B | | LINK C | |
|---|---|---|---|---|---|---|
| | ROLE | WT | ROLE | WT | ROLE | WT |
| Wave propagation | | | | | | |
| Antenna diagram | | | | | | |
| Low frequencies | | | | | | |
| Direction finding | | | | | | |
| Determination of rock parameters | | | | | | |
| Magnetic dipole antenna and receiver | | | | | | |
| Theoretical curves of wave propagation | | | | | | |
| Methods of direction finding | | | | | | |